An atypical ABC transporter is involved in antifungal resistance and host interactions in the pathogenic fungus *Cryptococcus neoformans*

Christopher J. Winski[a], Yuanyuan Qian[b], Shahriar Mobashery[b], Felipe H. Santiago-Tirado[a#]

[a]Department of Biological Sciences, Eck Institute for Global Health, University of Notre Dame, Notre Dame, IN 46656

[b]Department of Chemistry and Biochemistry, Warren Center for Drug Discovery, University of Notre Dame, Notre Dame, IN 46656

Running Head: A PDR transporter with dual roles in *C. neoformans*

[#]Address correspondence to Felipe H. Santiago-Tirado, fsantiago@nd.edu

Word Counts

Abstract: 242

Importance: 148

Text: 6667

ABSTRACT

ATP-binding cassette (ABC) transporters represent one of the largest protein superfamilies. Functionally diverse, ABC transporters have been implicated in many aspects of microbial physiology. The genome of the human fungal pathogen *Cryptococcus neoformans* encodes 54 putative ABC transporters and the majority of them remain uncharacterized. In a previous genetic screen for fungal regulators of phagocytosis, we identified an uncharacterized gene, CNAG_06909, that modulates host interactions. This gene encodes a half-size ABC transporter of the PDR-type, and phenotypic studies of a strain with this gene deleted revealed an altered antifungal susceptibility profile, including hypersensitivity to fluconazole (FLC). This gene, which we have named *PDR6*, localizes to the endoplasmic reticulum (ER) and plasma membrane (PM), and when absent, less ergosterol is observed in the PM. Additionally, we observed that the *pdr6*Δ strain displays a reduction in secreted polysaccharide capsular material. These changes to the cellular surface may explain the observed increased uptake by macrophages and the reduced intracellular survival. Finally, studies in mice demonstrate that Pdr6 function is required for normal progression of cryptococcal infection. Taken together, this study demonstrates a novel dual role for PDR transporters in *C. neoformans*, which could represent a potential target for antifungal therapeutics. Furthermore, the atypical half-size transporter encoded by *PDR6* is conserved in many fungal pathogens, but absent in model non-pathogenic fungi. Hence, this study provides for the first time, a function for this unique group of fungal half-size PDR transporters that, although conserved, remain largely understudied.

IMPORTANCE

Conserved across all kingdoms of life, ABC transporters comprise one of the largest protein families. They are associated with multidrug resistance, affecting aspects such as resistance to antimicrobials or anti-cancer drugs. Despite their importance, they are understudied in fungal pathogens. In the

47 environmental fungus *Cryptococcus neoformans*, a leading cause of fungal infections, only a few ABC
48 transporters have been studied. Here we characterize an atypical, half-size, ABC transporter of the PDR-
49 type, that affects both antifungal resistance and host-pathogen interactions. PDR-type transporters are
50 only present in fungi and plants, and this subgroup of half-size transporters is conserved in fungal
51 pathogens, yet their function was completely unknown. Because the current treatments for
52 cryptococcal infection are suboptimal, understanding the mechanisms of antifungal resistance and the
53 host interactions that drive the infection is critical to improve the management of this disease. Here we
54 provide insights into these important aspects of cryptococcal pathogenesis.
55

56 **INTRODUCTION**

57 Present in every living organism, ATP-binding cassette (ABC) transporters constitute a large
58 superfamily of integral membrane proteins. Functionally, ABC transporters are responsible for the
59 transport of diverse substrates across membranes, but have also been implicated in mRNA translation
60 and peroxisome biogenesis (1, 2). Structurally, ABC transporters contain at least one nucleotide-binding
61 domain (NBD) and one transmembrane domain (TMD), both of which are evolutionary conserved. Most
62 ABC transporters have a domain arrangement of TMD1-NBD1-TMD2-NBD2 ($[TMD\text{-}NBD]_2$) (3). The
63 orientation and molecular architecture of these domains is used to organize ABC transporters into
64 subgroups. The pleiotropic drug resistance (PDR) subgroup, which is present in only fungi and plants, has
65 a reverse configuration $[NBD\text{-}TBD]_2$ (4, 5). Identified and predominantly studied in the non-pathogenic
66 yeast *Saccharomyces cerevisiae*, they remain understudied in pathogenic fungi. This is despite the
67 abundance of fungal PDR proteins and the fact that fungal infections globally kill close to 1.6 million
68 people yearly (6, 7). The few that have been studied mostly act as efflux pumps for xenobiotics,
69 including antifungal drugs. Nonetheless, the sheer number and diversity of PDR genes found in fungal
70 genomes suggests a broad involvement in cellular processes. Moreover, there is a subgroup of half-size

71 PDR transporters (containing only one NBD and TMD) whose function remains unknown. Because all
72 functional PDR transporters studied so far have the typical [NBD-TBD]$_2$ domain arrangement, these half-
73 size ABC transporters with a [NBD–TMD] topology have been left out of PDR protein phylogenetic
74 studies (4, 5, 8).

75 *Cryptococcus neoformans* is an environmental, opportunistic fungal pathogen responsible for
76 over 180,000 deaths annually in the HIV+ population alone (9, 10). Upon inhalation and subsequent lung
77 colonization, *C. neoformans* can disseminate to the central nervous system (CNS) resulting in
78 cryptococcal meningitis, with a mortality rate as high as 81% (10). The high mortality rate is a direct
79 consequence of the complexities associated with cryptococcal pathogenesis coupled with a paucity of
80 effective antifungals. Currently, the most effective treatment for cryptococcal meningitis includes a
81 combinatorial regimen of amphotericin B (AMB) and 5-flucytosine (5-FC). AMB is a fungicidal polyene
82 that targets ergosterol, an essential lipid in the fungal plasma membrane (PM). The pyrimidine 5-FC
83 disrupts DNA/RNA synthesis (11). Notwithstanding toxicity associated with these agents, they are also
84 costly, which makes them less available to resource-poor countries, where the need is highest. Instead,
85 patients in these regions are treated with the less effective fluconazole (FLC) monotherapy. FLC is a
86 fungistatic azole that inhibits lanosterol 14α-demethylase, an enzyme in the ergosterol biosynthesis
87 pathway encoded by *ERG11* (12). FLC monotherapy has not only been implicated in higher relapse rates,
88 but several recent studies have reported an increase in the incidence of FLC resistance in *C. neoformans*,
89 making the treatment of cryptococcal meningitis even more challenging (13-16).

90 Several FLC resistance mechanisms have been reported in *C. neoformans*. These vary from
91 mutations in the *ERG11* gene to heteroresistance due to genome plasticity including polyploidy,
92 aneuploidy, loss of heterozygosity, and copy-number variation (17-20). Additionally, the overexpression
93 of ABC efflux pumps has been implicated in FLC resistance (21). There are 54 putative ABC transporters
94 in the *C. neoformans* genome and only a few have been characterized. The roles of *C. neoformans AFR1*,

95 *PDR5* (also called *AFR2*), and *MDR1* as azole efflux pumps have been well documented, where *AFR1*
96 functions as the major pump and *AFR2* and *MDR1* provide additive roles in the management of FLC
97 stress (22-25). It is evident that the function of most of the ABC transporters encoded in the *C.*
98 *neoformans* genome remain unknown. In an earlier report on fungal regulators of phagocytosis, we
99 identified an uncharacterized gene, CNAG_06909, as a modulator of the fungal-host interaction (26). In
100 the present study, we demonstrate that CNAG_06909 encodes a half-size PDR-transporter and that
101 disruption of the gene results in hypersensitivity to FLC. Following nomenclature guidelines for the field
102 (27), we have designated the gene as pleiotropic drug resistance-6 (*PDR6*) because it does not have a
103 direct ortholog in the model yeast *S. cerevisiae* and the molecular architecture is consistent with the
104 PDR subgroup of ABC transporters (see Supplemental Text S1 for more details). We show that Pdr6 does
105 not function as a FLC efflux pump but its deletion results in decreased levels of ergosterol in the PM,
106 accompanied by mild thermosensitivity and decreased secretion of capsular material. These phenotypes
107 are unique to *PDR6* as they were not observed in the previously characterized ABC transporters.
108 Furthermore, the *pdr6*Δ strain exhibits diminished intracellular survival *in vitro* and is attenuated in a
109 murine model of infection. When the gene is expressed in model yeast, it localizes to the ER and PM,
110 consistent with a role in ergosterol synthesis/transport. Notably, this study provides for the first time a
111 function for the group of unconventional, yet conserved, half-size PDR transporters, which has remained
112 largely obscure. These studies highlight the importance of fungal PDR-type transporters and broaden
113 our understanding of the specialization of ABC transporters in microbial pathogens.
114

115 **RESULTS**

116 ***C. neoformans PDR6* is a member of a conserved group of half-size PDR transporters**

117 Present in only fungi and plants, PDR-type ABC transporters represent a unique subset of proteins
118 primarily implicated in drug resistance and detoxification (4). Although fungal PDR-type transporters

119 closely resemble mammalian ABCG transporters, which are half-size, only the full-size fungal PDR
120 proteins have been analyzed and studied (5, 8, 28). Given that *C. neoformans PDR6* is half-size, we
121 performed a phylogenetic analysis to determine how widespread *PDR6* sequences are in the fungal
122 kingdom (Fig. 1A). All fungi belonging to the Pezizomycotina subphylum and all the pathogenic fungi
123 analyzed have a *PDR6* ortholog, implicating *PDR6* in fungal pathogenesis in many subphyla. Regardless
124 of the presence of a *PDR6* ortholog, all the PDR-type ABC transporter genes from the organisms in
125 Figure 1A were used to construct a global phylogenetic tree (Fig. 1B). Analysis of the fungal PDR genes
126 showed the presence of seven major clades. Clade I is the largest and includes *S. cerevisiae PDR5*,
127 *PDR10*, *PDR15*, and *C. neoformans PDR5* (hereafter referred by its alias *AFR2)*. Clade II is the smallest
128 and contains sequences that are homologous to *S. cerevisiae PDR12*, *PDR18* and *SNQ2.* Clade III
129 sequences are absent in Saccharomycotina, but contain *C. neoformans AFR1*. *S. cerevisiae PDR11* and
130 *AUS1* represent the genes in clade IV. Clades I, II, III, IV, and VIa all contain full-length *PDR* genes,
131 whereas clades V and VIb represent atypical groups of PDR genes that only encode one nucleotide-
132 binding domain (NBD) and one transmembrane domain (TMD). *S. cerevisiae ADP1* is representative of
133 the genes in clade V that all contain a NBD and TMD with an additional unique sequence (most
134 commonly an EGF domain). *C. neoformans PDR6* and the eleven other half-size PDR genes in clade VIb
135 represent a completely uncharacterized group of fungal genes with no known function. Interestingly,
136 the fungi represented in clade VIb are all plant or animal pathogens, again suggestive that *PDR6* and its
137 orthologs may be implicated in fungal virulence. Topology prediction by CAMPS (29) shows that *C.*
138 *neoformans PDR6* encodes a 626 amino acid half-size transporter, with a single NBD containing
139 characteristic Walker A, Walker B, and ABC motif features followed by a single TMD, composed of six
140 transmembrane helices (Fig. 1C). These analyses show that *C. neoformans PDR6* encodes a half-size PDR-
141 type ABC transporter that is evolutionarily conserved, with orthologs present in all fungal pathogens
142 that we analyzed, and contains all the features of a functional ABC transporter.

143

144 **Deletion of *PDR6* affects resistance to azoles and the drug profile of other antifungals**

145 Given that cryptococcal PDR-type ABC transporters Afr1 and Afr2 have been implicated in the efflux and
146 resistance of antifungal compounds (23-25), we hypothesized that Pdr6 would function in a similar
147 manner. To assess the function/specificity of Pdr6, we used a *C. neoformans* strain lacking the *PDR6*
148 gene (*pdr6*Δ) and tested its growth on FLC gradient plates and Etest strips (Fig. 2A), and performed broth
149 microdilution assays to measure the minimal-inhibitory concentrations (MICs) of several related
150 compounds (Fig. 2B-G and Table 1). Compounds included five azole-class antifungals (FLC, itraconazole
151 (ITC), voriconazole (VRC), ketoconazole (KTC), and posaconazole (PSC)), one polyene-class antifungal
152 (amphotericin B (AMB)), one DNA/RNA synthesis inhibitor (5-fluorocytosine (5-FC)), one protein-
153 synthesis inhibitor (cycloheximide (CHX)), one antineoplastic agent (nocodazole), two other xenobiotics
154 (berberine (BER), and paraquat (PQ)), one superoxide generator (menadione), and one echinocandin-
155 class antifungal (caspofungin (CSF)). In addition to the *pdr6*Δ mutant strain, we used the *afr1*Δ,
156 *afr1*Δ/*afr2*Δ/*mdr1*Δ, and *erg3*Δ strains as controls, since all have displayed increased FLC susceptibility
157 (24, 30).

158 Among the compounds tested, we found that the *pdr6*Δ mutant displayed a hypersensitive
159 phenotype specifically towards the azole class antifungals, albeit not as drastic as the *afr1*Δ,
160 *afr1*Δ/*afr2*Δ/*mdr1*Δ, or *erg3*Δ strains (Fig. 2 and Table 1). The MICs of the non-azole compounds in the
161 *pdr6*Δ strain were comparable to those of the H99 WT, suggesting a specific role of Pdr6 in azole
162 resistance. Additionally, previous studies have shown a relationship between environmental pH and
163 antifungal efficacy (31), so we performed FLC susceptibility assays at alkaline and acidic conditions (Fig.
164 S1A,B). Regardless of the pH, the MICs of the WT and *pdr6*Δ strains displayed similar trends indicating
165 that *PDR6* functions in a pH-independent manner.

166 Given the increase in azole susceptibility by the *pdr6*Δ mutant, we performed checkerboard
167 assays with four common antifungals, FLC, AMB, 5-FC, and CSF (Fig. 3). Interestingly, we found that FLC
168 coupled with CSF functions differently in the *pdr6*Δ strain when compared to the WT. The combination
169 works strongly in an additive manner in the *pdr6*Δ strain but shows minimal combinatorial effects in the
170 WT. This finding was unexpected given that CSF is ineffective at treating cryptococcal infections.
171 Additional experimentation is required to explain the observed finding. Nonetheless, these data show
172 that *PDR6* is involved in azole resistance, is not affected by pH, and can alter antifungal combinatorial
173 behaviors. All of these results were confirmed using three independently recreated *pdr6*Δ mutants (Fig.
174 S1C and Materials and Methods).
175
176 **Deletion of *PDR6* does not affect drug accumulation**
177 The increased azole susceptibility of the *pdr6*Δ mutant led us to hypothesize that Pdr6 could function as
178 an efflux pump, similar to many of the characterized fungal PDR transporters. Rhodamine 6G (R6G) and
179 Nile Red (NR) are fluorescent xenobiotics that have been used as generic probes to measure ABC
180 transporters' efflux activity (32, 33). To determine if Pdr6 functions as an efflux pump, we measured the
181 intracellular accumulation of R6G and NR by flow cytometry (Fig. 4A). Surprisingly, no difference was
182 observed in the mean fluorescent intensity (MFI) values of either R6G or NR in the *pdr6*Δ mutant,
183 compared to the WT. In contrast, the *afr1*Δ and *afr1*Δ/*afr2*Δ/*mdr1*Δ strains accumulated high levels of
184 these xenobiotics. We reasoned that Pdr6 may not recognize R6G or NR and potentially, Pdr6 is strictly
185 an azole-specific transporter. To test this, we synthesized a dansyl amide labeled-FLC molecule, termed
186 Probe 1 (Fig. 4B, left), that has been used to visualize the intracellular localization of FLC in *Candida*
187 *albicans* (34). Although the modification of FLC with dansyl amide affected its antifungal activity, the
188 strains more sensitive to FLC were also more sensitive to Probe 1, indicating a similar mechanism of
189 action (Fig. 4B, right). Consistently, the intracellular accumulation of Probe 1 was significantly increased

190 in the *afr1*Δ and *afr1*Δ/*afr2*Δ/*mdr1*Δ strains (Fig. 4C). However, there was no difference in the
191 intracellular accumulation of Probe 1 between the *pdr6*Δ strain and WT, suggesting that Pdr6 is not a
192 major efflux pump for FLC and instead affects azole activity by a different mechanism. We also used light
193 microscopy to assess the intracellular localization and accumulation/fluorescent intensity of Probe 1
194 between strains and no differences in location were observed, while fluorescent intensity values
195 supported the findings above (data not shown). To provide definitive support that Pdr6 is not acting as a
196 FLC-specific efflux pump, we directly measured accumulation of FLC using a liquid chromatography-mass
197 spectrometry (LC-MS)-based FLC accumulation assay (Fig. 4D). We found that the *pdr6*Δ mutant once
198 again displayed levels comparable to the WT, while the *afr1*Δ/*afr2*Δ/*mdr1*Δ positive control strain
199 accumulated significant amounts of FLC. Taken together, these data support that Pdr6 is not functioning
200 as a drug-efflux pump and that the hypersensitivity to azole antifungals in the *pdr6*Δ strain is not due to
201 increased accumulation of these drugs.
202
203 ***PDR6* is involved in ergosterol trafficking**
204 To mechanistically explain Pdr6's contribution to antifungal resistance, we next considered azoles' mode
205 of action. It is well documented that the target of azoles is Erg11, an enzyme in the ergosterol
206 biosynthesis pathway (18, 35). Disruptions to the ergosterol metabolic pathway can result in
207 accumulation of sterols, which have been implicated in both diminished and increased effectiveness of
208 azole compounds (30, 36). We, therefore, hypothesized that the azole resistance phenotype might be a
209 result of *Pdr6*'s involvement in ergosterol transport. To quantify ergosterol content in the cryptococcal
210 PM, we used filipin, a sterol-binding fluorescent dye (Fig. 5). We found a significant difference in
211 fluorescence between the WT and the *pdr6*Δ mutant. Specifically, the deletion of *PDR6* resulted in
212 decreased fluorescence, suggesting that less sterol is present and that Pdr6 plays a role in either the
213 synthesis of sterols or their trafficking; ABC transporters have been implicated in the latter (1, 37, 38),

214 supporting a potential role for Pdr6 in ergosterol transport to the PM. Notably, neither the *afr1*Δ nor
215 *afr1*Δ/*afr2*Δ/*mdr1*Δ strains exhibited reductions in filipin staining, indicating that the reduced sterol is
216 specific for *pdr6*Δ. As a control, we used *erg3*Δ strain, which is expected to have low levels of ergosterol
217 and, consistently, had almost no detectable staining. We further corroborated the quantitative
218 microscopy results using a fluorescent plate reader, confirming that the *pdr6*Δ mutant has reduced
219 overall ergosterol, compared to the WT (data not shown). These findings provide context for the
220 previously observed antifungal phenotype and demonstrate that the *pdr6*Δ strain has an altered PM
221 with less ergosterol, consistent with a role of *PDR6* in ergosterol transport/trafficking. Lastly, an indirect
222 role of *PDR6* in azole resistance is supported by the fact that the presence of FLC does not affect the
223 expression of *PDR6* (Fig. S2A), while growth under host-like conditions (DMEM, 37 °C, 5% CO_2) induce a
224 rapid and sustained increase in transcript levels (Fig. S2B). Ergosterol is essential for thermotolerance
225 and survival inside mammalian hosts (38), so if *PDR6* is involved in ergosterol transport, then it would be
226 expected to be overexpressed under host-like conditions.
227
228 **Pdr6 localizes to the ER and PM**
229 To better understand the function of Pdr6, we generated a C-terminally tagged *PDR6*-GFP integrative
230 construct under the control of the *PDR5* promoter and introduced it into the *S. cerevisiae* strain ADΔΔ
231 (39, 40). This strain is missing seven major endogenous ABC transporters and expresses a mutant Pdr1
232 transcription factor, driving overexpression of PDR genes. This strain not only allows for the visualization
233 of Pdr6 localization, but also a more direct assessment of efflux activity, provided cryptococcal Pdr6
234 would be the only major PDR protein in the cell. Visualization of the ADΔΔ+Pdr6-GFP strain revealed
235 clear perinuclear and peripheral staining, characteristic of the yeast endoplasmic reticulum (ER) (Fig.
236 6A). Similarly, a control ADΔΔ strain expressing Afr1-GFP, a full-length PDR-type transporter, displayed

237 comparable localization patterns consistent with the ER and PM (Fig. 6A). No GFP fluorescence was seen
238 in the strain transformed with an empty vector (Fig. 6A).
239
240 ***PDR6* expression does not restore efflux activity but increases sterol staining in the ADΔΔ strain.**
241 Using the same set of strains as above, we measured FLC susceptibility with Etest strips. The strain
242 expressing Afr1-GFP, a known FLC efflux pump, exhibited a 12-fold increase in MIC (MIC = 0.75 µg/mL)
243 over the ADΔΔ+empty vector control (MIC = 0.064 µg/mL; Fig. 6B). In contrast, the ADΔΔ+Pdr6-GFP
244 strain exhibited a modest increase with a MIC of 0.25 µg/mL, resulting in a 4-fold increase over the
245 control but a 3-fold decrease compared to the ADΔΔ+Afr1-GFP strain. If this small increase in MIC was
246 due to Pdr6-efflux activity, we should be able to measure it using the flow cytometry assay described
247 above. As shown in Fig. 6C, no differences were seen in the amounts of accumulated drugs between the
248 ADΔΔ+empty vector control and the strain expressing *PDR6*-GFP. In contrast, expression of *AFR1*-GFP
249 resulted in a significant decrease in the levels of R6G and Probe 1, albeit not to the levels seen in the WT
250 BY4741 control strain. The decrease in NR was not statistically significant, but a clear downward trend
251 was also observed in the ADΔΔ+Afr1-GFP strain. Next, given the filipin-staining results shown in Fig. 5,
252 we reasoned that the small MIC increase seen could be due to the potential role of Pdr6 in ergosterol
253 transport. To test this, we subjected the set of ADΔΔ strains to filipin staining and analysis as above.
254 Consistently, the ADΔΔ strains with an empty vector or expressing Afr1-GFP had the lowest PM
255 fluorescence, while the ADΔΔ+Pdr6-GFP had fluorescence that was indistinguishable from the WT
256 control (Fig. 6D). All of these results, together with the localization of Pdr6-GFP, suggest that the role of
257 Pdr6 in azole resistance stems from effects on ergosterol synthesis and/or transport and not from acting
258 as a specific FLC efflux pump.
259
260 ***PDR6* influences interaction with host macrophages**

261 Alveolar macrophages represent the first line of defense against cryptococcal infections and the
262 complex fungal-phagocyte interaction ultimately determines the course of infection and patient
263 outcome (41). We initially identified *PDR6* in a screen for fungal regulators of phagocytosis (26). We
264 used the same automated high-content imaging method to quantify the phagocytic index (PI) of the
265 library's *pdr6*Δ strain and the recreated strains by a human monocytic cell line (THP-1) (Fig. 7A and S1D).
266 In agreement, the original and recreated *pdr6*Δ mutants were all phagocytosed more readily than the
267 WT, providing evidence that changes in phagocytosis are a direct result of loss of *PDR6* function. The
268 *pka1*Δ strain served as a high-uptake positive control (26). This observation begs the question of how
269 the deletion of an atypical PDR-type ABC transporter was affecting the cryptococcal-host interaction.
270 We first tested if the absence of *PDR6* affected the cryptococcal capsule. The *pdr6*Δ mutant was able to
271 generate capsule comparable to the WT, indicating that *PDR6* is not involved in capsule formation (Fig.
272 S2C). Next, we assessed if there were any defects in cell-wall structure by growing *pdr6Δ*, WT, *afr1*Δ, and
273 *afr1*Δ/*afr2*Δ/*mdr1*Δ strains under cell-wall-stress conditions (Fig. S2D). All strains (except for *erg3*Δ)
274 grew under the tested conditions, and melanized normally, suggesting that there are no defects in the
275 cell wall (Fig. S2D,E). Finally, we hypothesized that *PDR6* was involved in the secretion/efflux of an
276 immunomodulatory factor and thus influencing host interactions. To test this idea, we performed similar
277 uptake assays as previously described, but used strain-specific conditioned media (CM) during the
278 cryptococcal-macrophage coincubation. The thought process being that if *PDR6* is in fact responsible for
279 the release of an immunomodulatory compound, then the CM from the *pdr6*Δ strain should influence
280 the uptake of the WT as to increase the PI values, whereas the CM from the WT should decrease the PI
281 values of the *pdr6*Δ strain. As shown in Fig. 7B, there were significant differences in phagocytosis
282 dependent on the source of the CM. Specifically, the incubation of the WT with *pdr6*Δ CM increased
283 uptake ~2-fold, while the incubation of the *pdr6*Δ strain with WT CM decreased uptake back to WT
284 levels. Notably, use of CM from the *afr1*Δ mutant had no significant impact on the PI values of either WT

285 or *pdr6*Δ strains. To test if this effect was specific for cryptococcal cells or impacted all phagocytic cargo,
286 we carried out the same assay with non-pathogenic *S. cerevisiae* (Fig. 7C). The host cells were able to
287 phagocytize a significant portion of this yeast regardless of the CM used. This suggests that *PDR6* is
288 involved in the release of an immunomodulatory factor that is present in the media and significantly
289 impacts phagocytosis of cryptococcal cells by host phagocytes. Taken together, these data confirm that
290 the *pdr6*Δ mutant is recognized and phagocytosed more avidly than the WT strain, and that the deletion
291 of *PDR6* alters the secretion/efflux of cryptococcal immunomodulatory compounds.
292
293 ***PDR6* is involved in capsular shedding and adherence**
294 To investigate in more detail how *PDR6* is altering the cryptococcal-phagocyte interaction, we focused
295 on the polysaccharide capsule. Primarily composed of glucuronoxylomannan (GXM) and
296 glucuronoxylomannogalactan (GXMGal), the capsule is known to be secreted/shed in a constitutive
297 manner. This secreted capsule plays a central role in virulence by acting as an antiphagocytic factor,
298 providing protection against host stressors, and modulating the host immune response (42, 43). We
299 wondered if the release/secretion of the capsule into the surrounding environment is altered in the
300 *pdr6*Δ mutant. To test this, we analyzed the amount of shed capsule by electrophoresis and
301 immunoblotting using anti-GXM antibodies (Fig. 8A) (44). Quantification of the immunoblots (Fig. 8A and
302 S2G) showed that the *pdr6*Δ mutant sheds less capsule compared to the WT in both DMEM and YNB
303 media, and this was significantly more pronounced in DMEM (Fig. 8A). Notably, there were no
304 differences in shed capsule between the *afr1*Δ, *afr1*Δ/*afr2*Δ/*mdr1*Δ, or *erg3*Δ strains and the WT,
305 indicating that this phenotype is unique to the Pdr6 transporter and not related to low levels of
306 ergosterol. The acapsular strain *cap59*Δ was used as a control. This observed defect in capsule shedding
307 could explain the phagocytosis phenotype, but to further test if there are functional consequences
308 associated with this defect, we performed biofilm/adherence assays (Fig. 8B). Previous studies have

309 shown that shed GXM is essential for the formation of cryptococcal biofilms (45-47). Consistently, we
310 found a similar trend where the *pdr6*Δ strain formed weaker/less biofilm structures when compared to
311 the WT, as measured by biomass quantification using anti-GXM antibody. Identical results were
312 obtained by metabolic quantification using XTT reduction assays (data not shown). Taken together,
313 these data suggest that *PDR6* is implicated in the shedding of the polysaccharide capsule, affecting both
314 phagocytosis by host cells and biofilm formation.
315
316 ***PDR6* function is required for *in vitro* and *in vivo* virulence**
317 Given the altered host interactions exhibited by the *pdr6*Δ mutant, its mild thermotolerance (Fig. S2F),
318 and the decreased capsule shedding, we next assessed its ability to survive within the challenging and
319 harsh intracellular environment. To test this, we performed *in vitro* survival assays and found that the
320 *pdr6*Δ mutant struggled to survive within host macrophages when compared to the WT (Fig. 9A). After
321 4h in the presence of naïve human macrophages, ~10% of intracellular WT cells died, whereas 25%-35%
322 of the *pdr6*Δ cells are killed. To expand on this mild *in vitro* defect, we tested the virulence of the *pdr6*Δ
323 mutant in a murine inhalation model of cryptococcosis, monitoring disease progression by weight loss.
324 Infection with the WT strain resulted in all animals steadily losing weight by about two weeks, 50% of
325 them dying in 17 days, and all succumbing to infection by day 19 (Fig. 9B). In contrast, mice infected with
326 the original *pdr6*Δ and the recreated *pdr6*Δ-1 strains lived about two weeks longer than the WT-infected
327 mice, with animals beginning to die at day 34, and all succumbing to infection by day 41, thus showing a
328 significant increase in survival. Notably, CFUs recovered from these mice at time of death showed
329 significantly less organ burden compared to WT-infected mice, and a clear defect in dissemination to
330 brain and spleen (Fig. 9C), supporting an altered progression or attenuated pathology. Consistently, the
331 *pdr6*Δ-infected mice exhibited respiratory symptoms (rapid and labored breathing) that were absent in
332 the WT-infected mice, and their lungs were significantly more inflamed and enlarged than the WT lungs

333 at time of death. Taken together, these data suggest that *PDR6* function is required for full cryptococcal
334 pathogenesis, and in its absence, the manifestation of the disease is protracted with altered
335 symptomatology.
336

337 **DISCUSSION**

338 The H99 genome contains 10 genes encoding PDR-type ABC transporters (Fig. 1B and Supplemental Text
339 S1). Although it has a conserved representative gene in all clades except clade II, few have been
340 characterized. Here we present an initial characterization of an atypical, half-size, PDR transporter found
341 in a fungal-host interaction screen. This gene, which we call *PDR6*, is conserved in the fungal kingdom
342 (clade VIb), but no function has been reported for that subgroup. Since all the other members of that
343 clade are pathogenic fungi, our work may have broad implication for medically-important fungi. Given
344 the similarity of *PDR6* to *AFR1* and *PDR5* (*AFR2*), which have been shown to act as efflux pumps for FLC,
345 we tested the hypothesis that *PDR6* might act in a similar way. However, our data show that it is unlikely
346 that Pdr6 is a major efflux pump for the compounds tested, including FLC. The *pdr6*Δ mutant
347 accumulates the same level of all these compounds, yet it is hypersensitive to them.

348 We then focused on ergosterol, the direct or indirect target of most antifungal drugs. Studies in
349 the model yeast *S. cerevisiae* have documented the ergosterol biosynthetic pathway in detail (48). This
350 occurs in the ER, yet how ergosterol is trafficked to the PM is not known, although it is known that
351 vesicular trafficking is not involved (49). In this yeast, *PDR18* has been implicated in that process, and
352 indeed, when *PDR6* is compared to the *S. cerevisiae* genome, *PDR18* is the gene closest to it, although
353 there is no real *PDR6* homolog in *S. cerevisiae*. Moreover, fungal and plant PDR genes are part of the
354 subfamily G of ABC transporters. In mammals, all ABCG members are half-size, and the mouse ABCG3
355 and human ABCG5 and 8 transporters are all involved in cholesterol transport (50). Interestingly, a
356 BLAST analysis of these ABCG sequences against the *Cryptococcus* genome identifies *PDR6* as the gene

357 with the highest similarity to ABCG3 and 8. Hence, our finding that Pdr6-GFP localizes to the ER and to
358 the PM, the biosynthesis site and final destination of ergosterol, respectively, and that the *pdr6*Δ mutant
359 has decreased ergosterol while the ADΔΔ+Pdr6-GFP increases PM ergosterol, strongly support a model
360 were Pdr6 functions as an ergosterol transporter. Notably, this function seems not to be conserved in
361 other PDR genes, as the *afr1*Δ and *afr1*Δ/*afr2*Δ/*mdr1*Δ mutants have normal levels of ergosterol as
362 quantified by filipin staining. Interestingly, the *pdr6*Δ mutant is not more resistant to AMB as would be
363 expected for strains lacking ergosterol (30), at least as judged by MIC values. A previous study of the
364 susceptibility of young and old cells to AMB found that cells lacking *PDR6* are less resilient to AMB
365 treatment, but this was measured as % survival and not as MIC values, preventing comparison of those
366 results with ours (51). Overall, our data indicate that the diminished levels of ergosterol are low enough
367 to promote sensitivity to azoles, but high enough to still be targeted by AMB and exert its antifungal
368 activity.

369 It is known that defects in the PM can affect the cell wall and/or capsule (52, 53). We did not
370 find evidence for gross alterations to either of these layers, but the defect in capsule shedding, and the
371 results of the CM studies, are highly suggestive of Pdr6 having a role in regulated shedding of the
372 capsule. It has been shown that capsule is shed constitutively, but recent studies have demonstrated
373 that capsule shedding can also be regulated (43). *PDR6* is highly and rapidly induced under host
374 conditions, which are conditions known to induce capsule growth and shedding. Notably, it is known
375 that normal levels of ergosterol are needed for thermotolerance, hence if *PDR6* is involved in ergosterol
376 homeostasis, it would be expected to be induced upon shift to body temperature. The altered ergosterol
377 levels in the *pdr6*Δ mutant could explain both the increased sensitivity to FLC and other azoles, and the
378 mild defect in thermotolerance (Fig. 10). However, low ergosterol cannot explain the reduced capsule
379 shedding in this mutant as the *erg3*Δ mutant, which also has low levels of ergosterol, sheds similar

380 amounts as WT. Additionally, other ergosterol mutants have also been shown to shed normal levels of
381 capsule (30). This phenotype still needs more investigation.

382 Lastly, we show that Pdr6 function is needed for normal progression and disease manifestation
383 in the mouse inhalational model. This could be explained by the decreased capsular shedding, high
384 phagocytosis, and lower intracellular survival (Fig. 10). The increased recognition and phagocytosis could
385 give the host an advantage since the fungus does not survive as well intracellularly. This would affect
386 dissemination, as there is ample evidence that phagocytes are needed for extrapulmonary
387 dissemination, a process known as trojan-horse transit (54). However, in order for trojan-horse transit to
388 occur, the fungus must be able to survive intracellularly, and the *pdr6*Δ mutant is defective in this
389 respect. Moreover, the decreased capsule shedding from the extracellular fungi would result in a
390 stronger inflammatory response. The *pdr6*Δ mutant is also capable of inducing production of a large
391 capsule, hence over time, less cells would be phagocytosed, and free cells in the tissue would
392 accumulate. With the increased fungal burden, and the stronger inflammatory response, the host
393 advantage is lost, and the animals die exhibiting different symptoms. Ongoing studies into the
394 immunological response of the animals to *pdr6*Δ infection will shed more light on this hypothesis.

395 In conclusion, we have described a new mechanism by which cryptococcal cells can modulate
396 their susceptibility to azoles: ergosterol transport regulated by Pdr6. Our results with the CM also
397 indicate a potential new antiphagocytic mechanism: the *pdr6*Δ mutant can still grow a capsule, yet it is
398 recognized and phagocytosed more avidly. Given that there are *PDR6* homologs in other fungal
399 pathogens, it would be interesting to see if this function is conserved. Notably, a *PDR6* ortholog is
400 missing in *C. deneoformans*, but present in *C. gattii*. *C. deneoformans* is considerably less pathogenic
401 than *C. neoformans,* and *C. gattii* is considered a primary pathogen, although it is more associated with
402 pneumonia than CNS infection. Would absence of *PDR6* in *C. deneoformans* contribute to the virulence
403 differences? Moreover, in addition to *PDR6*, *C. neoformans* has two additional half-size PDR

404 transporters, which are missing in *C. gattii*. These are not in clade VIb, but their function is nevertheless
405 unknown and could be related to Pdr6 since, in order to form a functional transporter, Pdr6 must homo-
406 or heterodimerize. The binding partner of Pdr6 might influence the function of the resulting complex,
407 which could be important under certain environmental conditions, such as inside a host. Elucidation of
408 the diverse functions of ABC transporters, specifically the PDR-type, has the potential to open new lines
409 of investigation for better treatments for this devastating disease.
410

411 **MATERIALS & METHODS**

412 **Strains, cell lines, growth conditions, and reagents**

413 All *C. neoformans* strains used were in the serotype A strain H99α background. The original *pdr6*Δ strain
414 was obtained from the Madhani deletion collection (55) and the recreated strains were made in this
415 background by biolistics (see below for details). H99α *afr1*Δ and H99α *afr1*Δ/*afr2*Δ/*mdr1*Δ were a
416 generous gift from Yun Chang (National Institutes of Health). The *S. cerevisiae* strain ADΔΔ and the
417 plasmids pABC3 and pABC3-KLmGH were graciously shared by Richard Cannon (Otago University, New
418 Zealand). Maintenance and growth conditions, as well as media details can be found in Supplemental
419 Text S1.

420 The human monocyte cell line THP-1 (ATCC TIB-202) was grown in THP-1 complete media and
421 differentiated with phorbol 12-myristate 12-acetate (PMA, Sigma) as described in (55). THP-1 cells were
422 split every 3-4 days and new vials were thawed every month. Details on complete media preparation
423 and differentiation into macrophages can be found in Supplemental Text S1.

424 All antifungals, xenobiotics, and other chemicals used were obtained through VWR or from
425 Sigma. Details on the preparation of stock solutions, including solvent concentrations, as well as their
426 storage information can be found in Supplemental Text S1.
427

428 **Fungal genome manipulation**

429 Since complementation strains of the original *pdr6*Δ (from the Madhani collection) proved challenging
430 to create, we used the split marker method (56) to delete the whole *PDR6* coding region in H99α after
431 amplifying NAT resistance split marker fragments from genomic DNA of strain 1F1 (*pdr6*Δ) of the
432 Madhani deletion collection. Three independent *pdr6*Δ mutant strains were generated to verify that all
433 observed phenotypes are a direct result of the loss of *PDR6* (Fig. S2). Additionally, we performed whole
434 genome sequencing on the generated *pdr6*Δ mutants to confirm proper genetic manipulation (data not
435 shown).

436

437 **Drug susceptibility assays**

438 The CLSI M27-A3 reference method was used to determine the MIC of each drug (57). Briefly, the
439 compounds to be tested were prepared at 2X the final concentration from stock solutions in RPMI 1640
440 medium. These were dispensed in a 96-well plate with 2-fold serial dilutions. 500 cells in the same
441 volume as the drugs were then added to each well. Plates were incubated at 37°C + 5% CO_2 for 48 – 72
442 hr. Minimal inhibitory concentrations (MICs) were quantified by measuring the OD_{600} using a microtiter
443 plate reader. For details on the compounds and concentration ranges tested see Supplemental Text S1.

444 The MIC of FLC was also determined on RPMI plates with Epsilometer test strips (Etest strips;
445 Liofilchem Thermo). Approximately 5 X 10^4 cells were plated on RPMI agar plates before application of
446 the Etest strips. Plates were incubated at 30°C for 48 hr.

447

448 **Checkerboard assays**

449 Checkerboard assays to assess the fractional inhibitory concentrations (FICs) for combinations of
450 antifungal drugs was performed as previously described (58). Log-phase cultures were used and mixed
451 with the antifungal stocks in RPMI 1640. For more details on the procedure, final antifungal

452 concentrations, and calculations of the FIC index, see Supplemental Text S1. A FIC index value of ≤ 0.5 is
453 considered synergistic, additive if the value is between 1.0 and 0.5, and antagonistic if the FIC index is ≥
454 2.0.
455

456 **Flow cytometry analysis of the efflux of R6G, Nile Red, and Probe 1**

457 Accumulation assays was performed as previously described (24, 34). Briefly, strains were grown
458 overnight in YPD at 30°C with shaking. Log-phase cultures were incubated with the fluorescent reporters
459 in PBS for 30 min at 30°C with shaking. The reactions were stopped by cooling on ice, and the mixture
460 was diluted 40-fold in cold 1X PBS. The accumulation was immediately assessed by flow cytometry. For
461 details on the concentration of the reporters, the lasers and filters used, and how the data was analyzed
462 see Supplemental Text S1. Synthesis of Probe 1 was done in the Mobashery lab following published
463 methods (34). For a detailed synthetic scheme and characterization of the product see Supplemental
464 Text S1.
465

466 **Liquid Chromatography/Mass Spectrometry (LC/MS)**

467 Log-phase cultures were incubated with FLC as above. A total of 200 µL was removed for CFU
468 quantification and the rest was processed to make the lysate. The lysate was mixed with same volume
469 of cold MeOH, vortexed, and spun down. The supernatant was mixed with the same volume of CH_2Cl_2,
470 vortexed, and spun down. The organic (bottom) phase was transferred into a glass tube, the solvent was
471 evaporated and the residues was resuspended in MeOH. At this point the samples were further cleaned
472 by passing through a solid-phase extraction (SPE) column. The elutes from SPE were concentrated by
473 speedvac, reconstituted in 50:50 water:MeOH, and analyzed using LC/MS. For details on the
474 instrumentation, columns, buffers, flow rates, software, and mass-spec parameters see Supplemental
475 Text S1.

476

477 **Phenotyping**

478 Strains tested were grown overnight in YPD, diluted to an OD_{600} of 0.2, and grown for two doublings. The
479 cultures were diluted to 1 x 10^7 cells/mL and serially diluted (10-fold) and spotted (5 µL) onto YPD with 1
480 M NaCl, 0.005% SDS, 0.1% Congo Red, and 0.5 µg/mL caffeine. Plates were incubated at 30ºC for 48 – 72
481 hr.

482

483 **Uptake Assay**

484 Uptake assays were performed as previously described (26). Briefly, differentiated THP-1 cells were
485 incubated with Lucifer Yellow-stained fungal cells that had been opsonized with 40% fresh human serum
486 obtained from healthy donors (approved by the UND IRB committee as a non-human subject research
487 procedure). Following a 1 hr incubation, the plates were washed using a microplate washer (405LS,
488 Biotek, Winooski, VT), fixed with 4% formaldehyde, and stained with DAPI (Sigma) and CellMask Deep
489 Red (Invitrogen). NaN_3 in PBS was added to the plates and images were obtained using a Zeiss Axio
490 Observer microscope, equipped with an automated stage. Each well was automatically imaged in a 3x3
491 grid and the images were analyzed using a Cell Profiler pipeline to determine phagocytic index (PI)
492 values. For more details on these procedures, including the Cell Profiler pipeline, see Supplemental Text
493 S1.

494

495 **Conditioned media**

496 Conditioned media (CM) was generated as previously described (59). Briefly, overnight cultures were
497 diluted to 1 X 10^5 cells/mL in RPMI 1640 media and incubated for 5 days at 30ºC. Cells were removed by
498 centrifugation and the supernatant was filtered through a 0.25-µm filter.

499

500 **Capsule induction**

501 Cells were grown overnight in YPD, washed with DMEM, and 1 X 10^6 cells/mL were added to 24-well
502 tissue culture plates. Plates were incubated at 37ºC + 5% CO_2 for 24 hr. Cell suspension was collected
503 and washed, India ink was added, and samples were visualized on a Zeiss microscope. Images were
504 analyzed with ImageJ (NIH) for capsule thickness.

505

506 **Capsule shedding assay**

507 Capsule shedding assays were performed as previously described (43, 44). Briefly, strains were grown
508 overnight in YPD at 30ºC, washed, and diluted to 1 X 10^6 cells/mL in DMEM. Following a 15 hr incubation
509 at 37ºC + 5% CO_2, the samples were heated to denature enzymes, centrifuged to separate cells and
510 supernatant, and then stored at 4ºC. The samples were loaded on a 0.6% certified megabase agarose
511 (Bio-Rad) gel and subjected to electrophoresis for 15 hr at 25 V. Gel contents were transferred to a
512 positively charged membrane using a standard Southern blot protocol with 10X SSC. Following overnight
513 transfer, the membrane was blocked for 48 hr in 1X TBS-5% milk and incubated for 1 hr in 1X TBST-1%
514 milk with 1 μg/mL of anti-GXM monoclonal antibody. Membrane was rinsed three times in 1X TBST and
515 incubated for 1 hr in 1X TBST-1% milk with Odyssey antibody at 1:10,000. Membrane was rinsed again
516 three times in 1X TBST and imaged on the Odyssey (Licor).

517

518 **Biofilm/Adherence assay**

519 Cryptococcal adherence assays were performed in nontreated 96-well plates (CLS3631, Corning). Briefly,
520 strains were grown overnight in YPD, diluted to 1 X 10^7 cells/mL in DMEM, and 100 μl of cell suspension
521 was added to the wells. Plates were incubated at 37ºC + 5% CO_2 for 72 hr, washed with PBS, fixed with
522 4% formaldehyde, blocked with 1.5% BSA and 0.1% NaN_3 in PBS, and incubated with anti-GXM primary

523 and secondary antibodies. Plates were imaged on the Odyssey and quantified using ImageStudio
524 software.
525 Biofilms were also quantified by the XTT reduction assay, as previously described (60, 61). For details on
526 this assay see Supplemental Text S1.
527

528 **Filipin staining**

529 Staining of membrane sterols was performed as previously described (36, 62). Briefly, log-phase cultures
530 grown in YPD were stained for 5 min with 5 µg/mL of filipin (Sigma) and washed with PBS. After washing
531 cells were immediately visualized with an inverted Zeiss microscope. Fluorescence was calculated using
532 Cell Profiler software. Additionally, fluorescent levels were quantified with a fluorescent plate reader
533 (Bio-Tek). Fluorescence was measured at the range of 360 to 470 nm wavelength and normalized by
534 OD_{600}.
535

536 **Mouse virulence studies**

537 To test virulence in a murine model, strains were cultured overnight in YPD, collected, washed, and
538 diluted to 10^6 cells/mL in DPBS. 50 µL of the cell suspension (or DPBS for the mock-infected) was used to
539 intranasally inoculate groups of five mice (5 to 6-week-old female A/Jcr mice; Jackson Laboratories).
540 Animals were closely monitored and sacrificed if they lost >20% relative to peak weight or at the end of
541 the experiment (41 days). Homogenates of lungs, brains, and spleens were plated to determine organ
542 burden.
543

544 **ACKNOWLEDGMENTS**

545 We acknowledge assistance and support for the LC-MS/MS by Dr. Mijoon Lee from the Notre Dame
546 Mass Spectrometry Core. We thank Dr. Richard Cannon for their gift of the ADΔΔ strain and associated

547 plasmids. We acknowledge financial support from the Warren Center for Drug Discovery for a Sean
548 Cocchia Rare Disease Research seed grant. We also thank members of the Santiago-Tirado lab for
549 thoughtful comments and feedback on this work.

550

551 **REFERENCES**

552 1. Higgins CF. 2001. ABC transporters: physiology, structure and mechanism--an overview. Res
553 Microbiol 152:205-10.
554 2. Jungwirth H, Kuchler K. 2006. Yeast ABC transporters-- a tale of sex, stress, drugs and aging.
555 FEBS Lett 580:1131-8.
556 3. Holland IB, Cole SPC, Kuchler K, Higgins CF. 2003. ABC Proteins from bacteria to man
557 doi:https://doi.org/10.1016/B978-0-12-352551-2.X5000-8. Academic Press, Amsterdam.
558 4. Khunweeraphong N, Kuchler K. 2021. Multidrug Resistance in Mammals and Fungi-From MDR to
559 PDR: A Rocky Road from Atomic Structures to Transport Mechanisms. Int J Mol Sci 22.
560 5. Lamping E, Baret PV, Holmes AR, Monk BC, Goffeau A, Cannon RD. 2010. Fungal PDR
561 transporters: Phylogeny, topology, motifs and function. Fungal Genet Biol 47:127-42.
562 6. Bongomin F, Gago S, Oladele RO, Denning DW. 2017. Global and Multi-National Prevalence of
563 Fungal Diseases-Estimate Precision. J Fungi (Basel) 3:57.
564 7. Niimi M, Tanabe K, Wada S, Yamazaki A, Uehara Y, Niimi K, Lamping E, Holmes AR, Monk BC,
565 Cannon RD. 2005. [ABC transporters of pathogenic fungi: recent advances in functional
566 analyses]. Nihon Ishinkin Gakkai Zasshi 46:249-60.
567 8. Kovalchuk A, Driessen AJ. 2010. Phylogenetic analysis of fungal ABC transporters. BMC
568 Genomics 11:177.
569 9. May RC, Stone NR, Wiesner DL, Bicanic T, Nielsen K. 2016. Cryptococcus: from environmental
570 saprophyte to global pathogen. Nat Rev Microbiol 14:106-17.
571 10. Rajasingham R, Smith RM, Park BJ, Jarvis JN, Govender NP, Chiller TM, Denning DW, Loyse A,
572 Boulware DR. 2017. Global burden of disease of HIV-associated cryptococcal meningitis: an
573 updated analysis. Lancet Infect Dis 17:873-881.
574 11. Coelho C, Casadevall A. 2016. Cryptococcal therapies and drug targets: the old, the new and the
575 promising. Cell Microbiol 18:792-9.
576 12. Zhang J, Li L, Lv Q, Yan L, Wang Y, Jiang Y. 2019. The Fungal CYP51s: Their Functions, Structures,
577 Related Drug Resistance, and Inhibitors. Front Microbiol 10:691.
578 13. Atim PB MD, Gerlach ES, Muhanguzi D, Male A, Kanamwanji B, Nielsen K. 2022. Lack of
579 Association between Fluconazole Susceptibility and ERG11 Nucleotide Polymorphisms in
580 Cryptococcus neoformans Clinical Isolates from Uganda. Journal of Fungi 8:508.
581 14. Hope W, Stone NRH, Johnson A, McEntee L, Farrington N, Santoro-Castelazo A, Liu X, Lucaci A,
582 Hughes M, Oliver JD, Giamberardino C, Mfinanga S, Harrison TS, Perfect JR, Bicanic T. 2019.
583 Fluconazole Monotherapy Is a Suboptimal Option for Initial Treatment of Cryptococcal
584 Meningitis Because of Emergence of Resistance. mBio 10.
585 15. Moreira IMB, Cortez ACA, de Souza ES, Pinheiro SB, de Souza Oliveira JG, Sadahiro A, Cruz KS,
586 Matsuura ABJ, Melhem MSC, Frickmann H, de Souza JVB. 2022. Investigation of fluconazole
587 heteroresistance in clinical and environmental isolates of Cryptococcus neoformans complex
588 and Cryptococcus gattii complex in the state of Amazonas, Brazil. Med Mycol 60.

589 16. Yang C, Bian Z, Blechert O, Deng F, Chen H, Li Y, Yang Y, Chen M, Zhan P. 2021. High Prevalence
590 of HIV-Related Cryptococcosis and Increased Resistance to Fluconazole of the Cryptococcus
591 neoformans Complex in Jiangxi Province, South Central China. Front Cell Infect Microbiol
592 11:723251.
593 17. Sionov E, Chang YC, Garraffo HM, Dolan MA, Ghannoum MA, Kwon-Chung KJ. 2012.
594 Identification of a Cryptococcus neoformans cytochrome P450 lanosterol 14alpha-demethylase
595 (Erg11) residue critical for differential susceptibility between fluconazole/voriconazole and
596 itraconazole/posaconazole. Antimicrob Agents Chemother 56:1162-9.
597 18. Rodero L, Mellado E, Rodriguez AC, Salve A, Guelfand L, Cahn P, Cuenca-Estrella M, Davel G,
598 Rodriguez-Tudela JL. 2003. G484S amino acid substitution in lanosterol 14-alpha demethylase
599 (ERG11) is related to fluconazole resistance in a recurrent Cryptococcus neoformans clinical
600 isolate. Antimicrob Agents Chemother 47:3653-6.
601 19. Bennett RJ, Forche A, Berman J. 2014. Rapid mechanisms for generating genome diversity:
602 whole ploidy shifts, aneuploidy, and loss of heterozygosity. Cold Spring Harb Perspect Med 4.
603 20. Stone NR, Rhodes J, Fisher MC, Mfinanga S, Kivuyo S, Rugemalila J, Segal ES, Needleman L,
604 Molloy SF, Kwon-Chung J, Harrison TS, Hope W, Berman J, Bicanic T. 2019. Dynamic ploidy
605 changes drive fluconazole resistance in human cryptococcal meningitis. J Clin Invest 129:999-
606 1014.
607 21. Holmes AR, Cardno TS, Strouse JJ, Ivnitski-Steele I, Keniya MV, Lackovic K, Monk BC, Sklar LA,
608 Cannon RD. 2016. Targeting efflux pumps to overcome antifungal drug resistance. Future Med
609 Chem 8:1485-501.
610 22. Posteraro B, Sanguinetti M, Sanglard D, La Sorda M, Boccia S, Romano L, Morace G, Fadda G.
611 2003. Identification and characterization of a Cryptococcus neoformans ATP binding cassette
612 (ABC) transporter-encoding gene, CnAFR1, involved in the resistance to fluconazole. Mol
613 Microbiol 47:357-71.
614 23. Sanguinetti M, Posteraro B, La Sorda M, Torelli R, Fiori B, Santangelo R, Delogu G, Fadda G.
615 2006. Role of AFR1, an ABC transporter-encoding gene, in the in vivo response to fluconazole
616 and virulence of Cryptococcus neoformans. Infect Immun 74:1352-9.
617 24. Chang M, Sionov E, Khanal Lamichhane A, Kwon-Chung KJ, Chang YC. 2018. Roles of Three
618 Cryptococcus neoformans and Cryptococcus gattii Efflux Pump-Coding Genes in Response to
619 Drug Treatment. Antimicrob Agents Chemother 62.
620 25. Ko YJ, Yu YM, Kim GB, Lee GW, Maeng PJ, Kim S, Floyd A, Heitman J, Bahn YS. 2009. Remodeling
621 of global transcription patterns of Cryptococcus neoformans genes mediated by the stress-
622 activated HOG signaling pathways. Eukaryot Cell 8:1197-217.
623 26. Santiago-Tirado FH, Peng T, Yang M, Hang HC, Doering TL. 2015. A Single Protein S-acyl
624 Transferase Acts through Diverse Substrates to Determine Cryptococcal Morphology, Stress
625 Tolerance, and Pathogenic Outcome. PLoS Pathog 11:e1004908.
626 27. Inglis DO, Skrzypek MS, Liaw E, Moktali V, Sherlock G, Stajich JE. 2014. Literature-based gene
627 curation and proposed genetic nomenclature for cryptococcus. Eukaryot Cell 13:878-83.
628 28. Velamakanni S, Wei SL, Janvilisri T, van Veen HW. 2007. ABCG transporters: structure, substrate
629 specificities and physiological roles : a brief overview. J Bioenerg Biomembr 39:465-71.
630 29. Neumann S, Hartmann H, Martin-Galiano AJ, Fuchs A, Frishman D. 2012. Camps 2.0: exploring
631 the sequence and structure space of prokaryotic, eukaryotic, and viral membrane proteins.
632 Proteins 80:839-57.
633 30. Oliveira FFM, Paes HC, Peconick LDF, Fonseca FL, Marina CLF, Bocca AL, Homem-de-Mello M,
634 Rodrigues ML, Albuquerque P, Nicola AM, Alspaugh JA, Felipe MSS, Fernandes L. 2020. Erg6
635 affects membrane composition and virulence of the human fungal pathogen Cryptococcus
636 neoformans. Fungal Genet Biol 140:103368.

637 31. Brown HE, Telzrow CL, Saelens JW, Fernandes L, Alspaugh JA. 2020. Sterol-Response Pathways
638 Mediate Alkaline Survival in Diverse Fungi. mBio 11.
639 32. Kolaczkowski M, van der Rest M, Cybularz-Kolaczkowska A, Soumillion JP, Konings WN, Goffeau
640 A. 1996. Anticancer drugs, ionophoric peptides, and steroids as substrates of the yeast
641 multidrug transporter Pdr5p. J Biol Chem 271:31543-8.
642 33. Ivnitski-Steele I, Holmes AR, Lamping E, Monk BC, Cannon RD, Sklar LA. 2009. Identification of
643 Nile red as a fluorescent substrate of the Candida albicans ATP-binding cassette transporters
644 Cdr1p and Cdr2p and the major facilitator superfamily transporter Mdr1p. Anal Biochem 394:87-
645 91.
646 34. Benhamou RI, Bibi M, Steinbuch KB, Engel H, Levin M, Roichman Y, Berman J, Fridman M. 2017.
647 Real-Time Imaging of the Azole Class of Antifungal Drugs in Live Candida Cells. ACS Chem Biol
648 12:1769-1777.
649 35. Paul S, Kannan I, Mohanram K. 2019. Extensive ERG11 mutations associated with fluconazole-
650 resistant Candida albicans isolated from HIV-infected patients. Curr Med Mycol 5:1-6.
651 36. Altamirano S, Simmons C, Kozubowski L. 2018. Colony and Single Cell Level Analysis of the
652 Heterogeneous Response of Cryptococcus neoformans to Fluconazole. Front Cell Infect
653 Microbiol 8:203.
654 37. Godinho CP, Prata CS, Pinto SN, Cardoso C, Bandarra NM, Fernandes F, Sa-Correia I. 2018. Pdr18
655 is involved in yeast response to acetic acid stress counteracting the decrease of plasma
656 membrane ergosterol content and order. Sci Rep 8:7860.
657 38. Godinho CP, Costa R, Sa-Correia I. 2021. The ABC transporter Pdr18 is required for yeast
658 thermotolerance due to its role in ergosterol transport and plasma membrane properties.
659 Environ Microbiol 23:69-80.
660 39. Lamping E, Monk BC, Niimi K, Holmes AR, Tsao S, Tanabe K, Niimi M, Uehara Y, Cannon RD.
661 2007. Characterization of three classes of membrane proteins involved in fungal azole resistance
662 by functional hyperexpression in Saccharomyces cerevisiae. Eukaryot Cell 6:1150-65.
663 40. Madani G, Lamping E, Lee HJ, Niimi M, Mitra AK, Cannon RD. 2021. Small-Scale Plasma
664 Membrane Preparation for the Analysis of Candida albicans Cdr1-mGFPHis. J Vis Exp
665 doi:10.3791/62592.
666 41. Gaylord EA, Choy HL, Doering TL. 2020. Dangerous Liaisons: Interactions of Cryptococcus
667 neoformans with Host Phagocytes. Pathogens 9.
668 42. Zaragoza O, Rodrigues ML, De Jesus M, Frases S, Dadachova E, Casadevall A. 2009. The capsule
669 of the fungal pathogen Cryptococcus neoformans. Adv Appl Microbiol 68:133-216.
670 43. Denham ST, Verma S, Reynolds RC, Worne CL, Daugherty JM, Lane TE, Brown JCS. 2018.
671 Regulated Release of Cryptococcal Polysaccharide Drives Virulence and Suppresses Immune Cell
672 Infiltration into the Central Nervous System. Infect Immun 86.
673 44. Yoneda A, Doering TL. 2008. Regulation of Cryptococcus neoformans capsule size is mediated at
674 the polymer level. Eukaryot Cell 7:546-9.
675 45. Martinez LR, Casadevall A. 2015. Biofilm Formation by Cryptococcus neoformans. Microbiol
676 Spectr 3.
677 46. Lee HH, Del Pozzo J, Salamanca SA, Hernandez H, Martinez LR. 2019. Reduced phagocytosis and
678 killing of Cryptococcus neoformans biofilm-derived cells by J774.16 macrophages is associated
679 with fungal capsular production and surface modification. Fungal Genet Biol 132:103258.
680 47. Ravi S, Pierce C, Witt C, Wormley FL, Jr. 2009. Biofilm formation by Cryptococcus neoformans
681 under distinct environmental conditions. Mycopathologia 167:307-14.
682 48. Jorda T, Puig S. 2020. Regulation of Ergosterol Biosynthesis in Saccharomyces cerevisiae. Genes
683 (Basel) 11.

684 49. Baumann NA, Sullivan DP, Ohvo-Rekila H, Simonot C, Pottekat A, Klaassen Z, Beh CT, Menon AK.
685 2005. Transport of newly synthesized sterol to the sterol-enriched plasma membrane occurs via
686 nonvesicular equilibration. Biochemistry 44:5816-26.
687 50. Kerr ID, Hutchison E, Gerard L, Aleidi SM, Gelissen IC. 2021. Mammalian ABCG-transporters,
688 sterols and lipids: To bind perchance to transport? Biochim Biophys Acta Mol Cell Biol Lipids
689 1866:158860.
690 51. Orner EP, Zhang P, Jo MC, Bhattacharya S, Qin L, Fries BC. 2019. High-Throughput Yeast Aging
691 Analysis for Cryptococcus (HYAAC) microfluidic device streamlines aging studies in Cryptococcus
692 neoformans. Commun Biol 2:256.
693 52. Kumar P, Heiss C, Santiago-Tirado FH, Black I, Azadi P, Doering TL. 2014. Pbx proteins in
694 Cryptococcus neoformans cell wall remodeling and capsule assembly. Eukaryot Cell 13:560-71.
695 53. Reese AJ, Doering TL. 2003. Cell wall alpha-1,3-glucan is required to anchor the Cryptococcus
696 neoformans capsule. Mol Microbiol 50:1401-9.
697 54. Santiago-Tirado FH, Doering TL. 2017. False friends: Phagocytes as Trojan horses in microbial
698 brain infections. PLoS Pathog 13:e1006680.
699 55. Liu OW, Chun CD, Chow ED, Chen C, Madhani HD, Noble SM. 2008. Systematic genetic analysis
700 of virulence in the human fungal pathogen Cryptococcus neoformans. Cell 135:174-88.
701 56. Fu J, Hettler E, Wickes BL. 2006. Split marker transformation increases homologous integration
702 frequency in Cryptococcus neoformans. Fungal Genet Biol 43:200-12.
703 57. CLSI. 2017. Reference Method for Broth Dilution Antifungal Susceptibility Testing of Yeasts. 4th
704 ed. CLSI Standard M27. Clinical and Laboratory Standard Institute, Wayne, PA.
705 58. Franzot SP, Casadevall A. 1997. Pneumocandin L-743,872 enhances the activities of
706 amphotericin B and fluconazole against Cryptococcus neoformans in vitro. Antimicrob Agents
707 Chemother 41:331-6.
708 59. Albuquerque P, Nicola AM, Nieves E, Paes HC, Williamson PR, Silva-Pereira I, Casadevall A. 2013.
709 Quorum sensing-mediated, cell density-dependent regulation of growth and virulence in
710 Cryptococcus neoformans. mBio 5:e00986-13.
711 60. Pierce CG, Uppuluri P, Tristan AR, Wormley FL, Jr., Mowat E, Ramage G, Lopez-Ribot JL. 2008. A
712 simple and reproducible 96-well plate-based method for the formation of fungal biofilms and its
713 application to antifungal susceptibility testing. Nat Protoc 3:1494-500.
714 61. Martinez LR, Casadevall A. 2005. Specific antibody can prevent fungal biofilm formation and this
715 effect correlates with protective efficacy. Infect Immun 73:6350-62.
716 62. Bang S, Kwon H, Hwang HS, Park KD, Kim SU, Bahn YS. 2014. 9-O-butyl-13-(4-
717 isopropylbenzyl)berberine, KR-72, is a potent antifungal agent that inhibits the growth of
718 Cryptococcus neoformans by regulating gene expression. PLoS One 9:e109863.

719

720

721 **FIGURE LEGENDS**

722

723 **FIG 1** *PDR6* contains all the features of a PDR-type ABC transporter and is conserved in a subset of fungal
724 pathogens. (A) Cladogram showing the fungal distribution of *PDR6* orthologs in the two main phyla.
725 When present, the gene name of the ortholog is stated within parentheses. (B) Global phylogenetic tree
726 showing the evolutionary relationships of PDR-type ABC transporters in 21 fungal organisms. Gene
727 names are given in NCBI nomenclature. Tree was generated by Maximum Likelihood Method using
728 MEGA-X and confidence values determined from 500 bootstraps with bootstrap scores shown at all
729 nodes. The tree shown is the bootstrap consensus tree. Analysis reveals VI major clades with *C.*
730 *neoformans PDR6* housed in clade VIb (denoted by dark green arrow). The 10 PDR-type transporters in
731 *C. neoformans* are in bold font and are listed in Supplementary Text S1. (C) Topology prediction of Pdr6
732 protein by Computational Analysis of the Membrane Protein Space (CAMPS) software showing the
733 domain arrangement of the half-size PDR transporter. The 5 main consensus motifs of the nucleotide
734 binding domain (NBD) are depicted.
735 The residues in green with a green 'Y' are predicted N-glycosylation sites.

736

737 **FIG 2** *PDR6* is involved in azole resistance. (A) The *pdr6*Δ mutant shows increased sensitivity to FLC
738 gradient plates and Etest strips. (Left) 500 cells of the indicated strains were spotted across a RPMI-1640
739 agar plate with a gradient of FLC concentration (denoted by black triangle). The gradient goes from near
740 zero at the left side to a peak concentration of 4 µg/mL at the right side of the plate. (Right) FLC Etest
741 strips were applied to RPMI-1640 agar plates with 2 x 10^5 cells of the indicated strain. The zone of
742 inhibition is highlighted with a dashed circle, and the MICs of H99 and the *pdr6*Δ mutant were 6 and
743 0.38 µg/mL, respectively. These plates were incubated for 72 hr at 30°C. (B-H) Quantitative broth
744 microdilution assays were used to compare MICs of several antifungal compounds in the WT and the

745 indicated mutant strains. The CLSI M27-A3 reference method was repeated three times for each
746 compound and the bars represent the average of the MICs. The details for each strain's MICs are listed
747 in Table 1. FLC, fluconazole; VRC, voriconazole; ITC, itraconazole; KTC, ketoconazole; PSC, posaconazole;
748 CHX, cycloheximide.
749
750 **FIG 3** Combinatorial FLC + CSF treatment have an additive effect in *pdr6*Δ mutant. Checkerboard assays
751 assessed changes in drug combinatorial activity in H99 and *pdr6*Δ strains. The combination of FLC + CSF
752 resulted in average sums of FIC of 1.083 and 0.625 in the H99 and *pdr6*Δ strains, respectively.
753 Calculations indicate an additive effect trending into synergistic in the absence of *PDR6*. Checkerboard
754 assays were repeated three times for each combination and black bars represent the average sum of
755 FIC.
756
757 **FIG 4** Deletion of *PDR6* does not affect intracellular accumulation of fluorescent reporters or of FLC. (A)
758 H99 and indicated deletion strains were incubated with 10 µM R6G or 7 µM NR for 30 min at 30ºC and
759 accumulation of the reporter in the cells was analyzed by flow cytometry as described in Materials and
760 Methods. (B) (Left) Chemical structure of Probe 1 with FLC backbone highlighted. (Right) Broth
761 microdilution assays were performed to compare the MICs of FLC with Probe 1. Regardless of strain, a
762 128-fold increase was observed in the MICs of Probe 1 when compared to FLC. Microdilution assays
763 were repeated three times and shown are the results from one representative experiment. (C) Indicated
764 strains were incubated with 10 µg/mL of Probe 1 and accumulation assessed by flow cytometry as
765 above. (D) Accumulation of FLC was assessed in H99 and deletion strains using LC-MS/MS. Strains were
766 incubated with 16 µg/mL of FLC for 30 min at 30ºC. All values represent the mean ± SEM from three to
767 four independent experiments. Significance was determined using one-way ANOVA compared to H99
768 (Brown-Forsythe and Welch's corrected); *P<0.05, **P<0.01, ****P<0.0001.

769

770 **FIG 5** *pdr6*Δ mutant displays reduced sterol content. (Left) To assess sterol content in WT and other
771 mutant strains, the cells were incubated with 5 µg/mL Filipin III for 5 min at 30ºC and visualized
772 microscopically. Scale bar, 5 µm. (Right) Quantification of fluorescence using a Cell Profiler pipeline.
773 Values represented are the mean ± SEM of 3 to 4 independent experiments where n=50 cells per
774 experiment. Significance was determined using one-way ANOVA with multiple comparisons (Brown-
775 Forsythe and Welch's corrected); *P<0.05, ***P<0.001.

776

777 **FIG 6** Pdr6 localizes to the ER and PM in *S. cerevisiae* but do not affect intracellular drug accumulation.
778 (A) Visualization of *S. cerevisiae* ADΔΔ expressing *C. neoformans PDR6*-GFP, *AFR1*-GFP, or empty vector.
779 DAPI staining was included to highlight the perinuclear staining. The GFP-tagged proteins localization is
780 consistent with the ER and PM. Scale bar, 3.8 µm. (B) Growth of the various ADΔΔ strains was assessed
781 using FLC Etest strips in RPMI plates. Strains expressing *PDR6* (MIC = 0.25 µg/mL) and *AFR1* (MIC = 0.75
782 µg/mL) display increased resistance to FLC compared to empty vector control (MIC = 0.064 µg/mL) but
783 the strain expressing *AFR1* was most resistant. Plates were incubated at 30ºC for 96 hr and imaged. The
784 zones of inhibition are highlighted with a dashed circle. (C) Accumulation of the indicated reporters was
785 assessed by flow cytometry as described in Fig. 4. There was no difference between the accumulated
786 drugs in the empty vector control and the strain expressing *PDR6*-GFP. Values represent the mean ±
787 SEM of at least 3 independent experiments. Significance was determined using one-way ANOVA with
788 multiple comparisons (Brown-Forsythe and Welch's corrected); **P < 0.01, ****P < 0.0001. (D)
789 Quantification of sterol content in transformed ADΔΔ strains and BY4741 control. The ADΔΔ + *PDR6*
790 displays increased filipin staining compared to the ADΔΔ control and ADΔΔ + *AFR1* but is
791 indistinguishable from the WT BY4741 strain. Log-phase cells were incubated with filipin and
792 imaged/quantified as described in Fig. 5. Values represent the mean ± SEM where n=50. Significance

793 was determined using one-way ANOVA with multiple comparisons (Brown-Forsythe and Welch's
794 corrected); **P < 0.01.
795
796 **FIG 7** The *pdr6*Δ mutant conditioned media (CM) increases the phagocytosis of other cryptococcal
797 strains by host macrophages. (A) Uptake assays of WT and deletion strains were performed to
798 determine phagocytic indices of respective strains. The *pdr6*Δ mutant displayed increased uptake
799 compared to the H99 strain. The *pka1*Δ cells were used as a positive control. Stained and opsonized log-
800 phase cells were incubated for 1 hr with THP-1 cells and imaged using automated microscopy. Values
801 represent the mean ± SEM from three independent experiments. (B) Uptake assay using CM from
802 cryptococcal strains was performed. CM obtained by centrifugation and filtration of supernatants from
803 5-day cultures incubated at 37°C + 5% CO_2 in RPMI-1640 media. The *pdr6*Δ CM altered the phagocytic
804 uptake values of the WT strain and vice versa, whereas the *afr1*Δ CM has no effect. Values represent the
805 mean ± SD of a representative experiment from three independent experiments. (C) Uptake assays with
806 CM were performed as in (B) but using *S. cerevisiae* strain BY4741. BY4741 is easily phagocytized by
807 THP-1 cells under all conditions. Significance was determined using one-way ANOVA with multiple
808 comparisons (Brown-Forsythe and Welch's corrected), *P<0.05; **P<0.01; ***P<0.001.
809
810 **FIG 8** Deletion of *PDR6* alters capsular secretion and biofilm formation. (A) Capsule shedding assays
811 were performed to determine amount of GXM secreted from cryptococcal strains into the media. (Left)
812 Representative immunoblot showing shed GXM from cells grown for 2 days in YNB. Visualization of shed
813 GXM was done using fluorescent detection (Odyssey, LiCor). Quantification of signal revealed that the
814 *pdr6*Δ mutant shed significantly less capsule than WT under DMEM (host-like) conditions and, albeit not
815 statistically significant, there was a clear trend of less shedding in YNB conditions as well. Values from at
816 least 3 independent experiments were normalized to the WT shed capsule and combined. Bars

817 represent the mean ± SEM. (B) Biofilm-forming assays were performed in nontreated microtiter plates,
818 incubated for 72 hr, washed, and visualized for biofilms using a fluorescent imaging system (Odyssey,
819 LiCor). Quantification of signal reveal that all *pdr6*Δ mutants form weaker/less adherent biofilms when
820 compared to the WT. Values from at least 3 independent experiments were normalized to WT and
821 combined. Bars represent mean ± SEM. Significance was determined using one-way ANOVA compared
822 to H99 (Brown-Forsythe and Welch's corrected); *P<0.05; ****P<0.0001.
823
824 **FIG 9** *pdr6*Δ mutant displays attenuated virulence *in vitro* and *in vivo.* (A) *In vitro* survival of H99 and
825 *pdr6*Δ strains. Fungi and THP-1 cells were coincubated for 1 hr at an MOI of 0.1, washed to remove free
826 cryptococci, and half the samples lysed to determine intracellular fungi and the other half grown for an
827 additional 3 hr, after which they were also lysed. Shown in % killed, values represent the mean ± SEM
828 from five independent experiments. Significance was determined using RM one-way ANOVA compared
829 to H99 (Geisser-Greenhouse correction); *P<0.05. (B) *In vivo* survival curve of H99 and *pdr6*Δ-infected
830 mice. Five to six AJ/Cr mice per group were infected intranasally with 5 x 10^4 *C. neoformans*, or mock
831 infected with DPBS and monitored for up to 41 days (experiment terminated when the last infected
832 mouse died). Significance was determined using Mantel-Cox test; ***P<0.001. (C) Calculated organ
833 burden of H99 and *pdr6*Δ strains at time of death. Organs were harvested, homogenized, and dilutions
834 were plated on YPD. Plates were incubated for 48 hr and CFUs counted. Each data point represents a
835 mouse and black bars represent the mean. There was significant less fungal burden in the lungs and a
836 clear defect in dissemination. Significance was determined using a nonparametric one-way ANOVA with
837 multiple comparisons (Dunn's corrected), *P<0.05.
838
839 **FIG 10** Model of Pdr6 and relationship to antifungal resistance, host interactions, and virulence. Pdr6 is a
840 half-size transporter (dark blue), hence it needs to dimerize with itself or another half-size transporter

841 (light blue) to be functional. In its absence, altered sterol content contributes to azole and thermal
842 susceptibility, and the reduced capsule shedding promotes recognition and phagocytosis by host
843 macrophages. Together, these phenotypes result in altered pathogenesis and attenuated virulence.
844
845 **TEXT S1** Supplemental methods and details on naming nomenclature for PDR genes in *C. neoformans*.
846
847 **FIG S1** Antifungal and phagocytosis phenotypes in original and recreated *pdr6*Δ mutant strains. (A)
848 Plates with FLC Etest strips to assess the zones of inhibition of H99 WT and *pdr6*Δ mutant cells grown on
849 standard (pH 5.5) or alkaline (pH 7.5) YNB medium. Regardless of pH, the *pdr6*Δ mutant was 4X more
850 susceptible than WT. The H99 and *pdr6*Δ mutant displayed FLC MICs of 64 and 16 µg/mL on the 5.5 pH
851 plates and 24 and 6 µg/mL under alkaline conditions. Plates were imaged after 72 hr of growth at 30ºC.
852 (B) MIC of FLC for H99 WT and *pdr6*Δ strains were determined by broth microdilution assays after 48 h
853 of growth at 30ºC in standard and alkaline YNB. Microdilution assays were repeated three times for each
854 condition and black bars represent the average MIC respectively. (C) Broth microdilution assays were
855 used to compare FLC MICs of three independently recreated *pdr6*Δ strains to the *pdr6*Δ strain from the
856 deletion collection. Assay was repeated three times and black bars represent the average MIC. (D)
857 Comparative phagocytic indices of the library and recreated *pdr6*Δ mutants with the H99 strain. All
858 *pdr6*Δ strains displayed significantly higher phagocytic values than the WT. Values represent the mean ±
859 SD of a representative experiment from three biological replicates. Statistical significance determined
860 using one-way ANOVA with multiple comparisons (Brown-Forsythe and Welch's corrected), *P<0.05,
861 **P<0.01.
862
863 **FIG S2** *PDR6* expression and virulence traits. (A) Transcript levels of *PDR6* in response to FLC exposure as
864 measured by qRT-PCR. Log phase cells were either untreated (control) or treated with 4 µg/mL of FLC for

865 2 hr. No significant difference was observed in the presence of the antifungal. Expression levels were
866 normalized to that of the actin gene. Values represent the mean ± SEM of three biological replicates. (B)
867 Data from an RNA-seq experiment to analyze expression levels of *PDR6* after shifting to host-like
868 conditions. Samples were taken prior to incubation (time = 0), and at 90, 180, 480, and 1,440 minutes
869 after. Expression increased almost 3-fold in the first 90 min and remained relatively high throughout 24
870 hr. (C) Capsule induction assays were performed to determine capsule thickness in cryptococcal strains.
871 Visualization and quantification of 24 hr cultures revealed that there was no significant difference in
872 capsule size between the H99 and *pdr6*Δ mutant. Scale bar, 5 µm. Values represent the mean ± SEM
873 where n=50. (D) Growth on stress plates was assessed to determine potential membrane or cell wall
874 defects in the indicated cryptococcal strains. No differences were observed in the *pdr6*Δ mutant. Mid-
875 log phase cultures were serially diluted on plates with cell wall/PM stressors and incubated for 72 hr at
876 30ºC. CR, Congo Red. (E) Melanization was assessed by appearance of pigmentation on caffeic acid
877 plates. 5.0 x 10^3 cells were spotted and incubated as above. (F) Thermotolerance was assessed by
878 spotting strains on YPD plates and incubating plates at 30 °C and 37 °C for 72 hr. A mild defect in growth
879 was observed in all the *pdr6*Δ mutants except *pdr6*Δ-3. (G) Representative immunoblot showing shed
880 GXM from cells grown for 24 hr in DMEM, 37 °C and 5% CO_2.

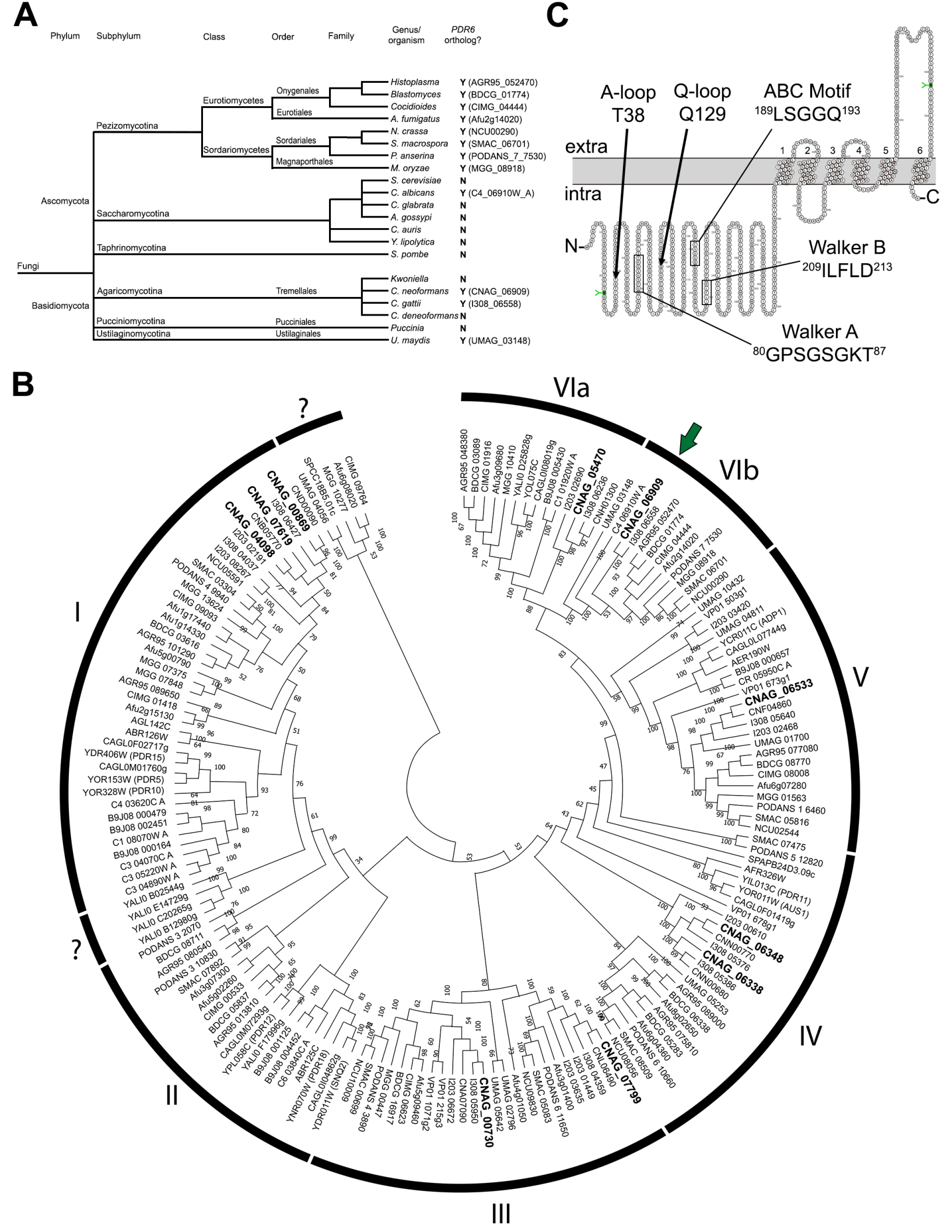
A
Phylum
Subphylum
Class
Order
Family
Genus/ organism
PDR6 ortholog?
Fungi
Ascomycota
Basidiomycota
Pezizomycotina
Saccharomycotina
Taphrinomycotina
Agaricomycotina
Pucciniomycotina
Ustilaginomycotina
Eurotiomycetes
Sordariomycetes
Onygenales
Eurotiales
Sordariales
Magnaporthales
Tremellales
Pucciniales
Ustilaginales
Histoplasma Y (AGR95_052470)
Blastomyces Y (BDCG_01774)
Cocidioides Y (CIMG_04444)
A. fumigatus Y (Afu2g14020)
N. crassa Y (NCU00290)
S. macrospora Y (SMAC_06701)
P. anserina Y (PODANS_7_7530)
M. oryzae Y (MGG_08918)
S. cerevisiae N
C. albicans Y (C4_06910W_A)
C. glabrata N
A. gossypi N
C. auris N
Y. lipolytica N
S. pombe N
Kwoniella N
C. neoformans Y (CNAG_06909)
C. gattii Y (I308_06558)
C. deneoformans N
Puccinia N
U. maydis Y (UMAG_03148)
C
A-loop T38
Q-loop Q129
ABC Motif
189LSGGQ193
extra
intra
1 2 3 4 5 6
N-
-C
Walker B
209ILFLD213
Walker A
80GPSGSGKT87
B
VIa
VIb
V
IV
III
II
I
?
?
CNAG_05470
CNAG_06909
CNAG_06533
CNAG_06348
CNAG_06338
CNAG_07799
CNAG_00730
CNAG_00869
CNAG_07619
CNAG_04098

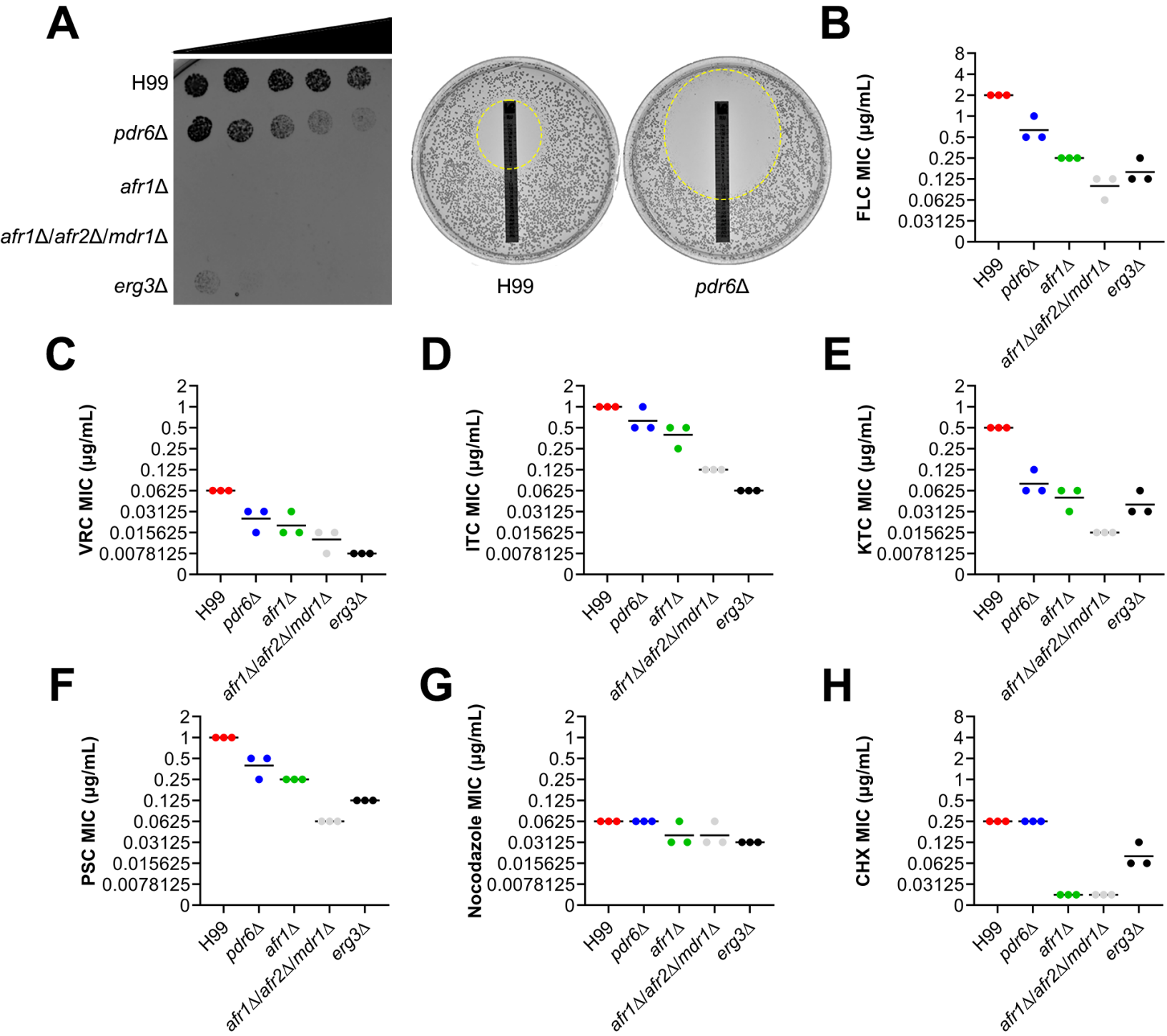
A
H99
pdr6Δ
afr1Δ
afr1Δ/afr2Δ/mdr1Δ
erg3Δ
H99
pdr6Δ
B
FLC MIC (µg/mL)
C
VRC MIC (µg/mL)
D
ITC MIC (µg/mL)
E
KTC MIC (µg/mL)
F
PSC MIC (µg/mL)
G
Nocodazole MIC (µg/mL)
H
CHX MIC (µg/mL)
H99
pdr6Δ
afr1Δ
afr1Δ/afr2Δ/mdr1Δ
erg3Δ

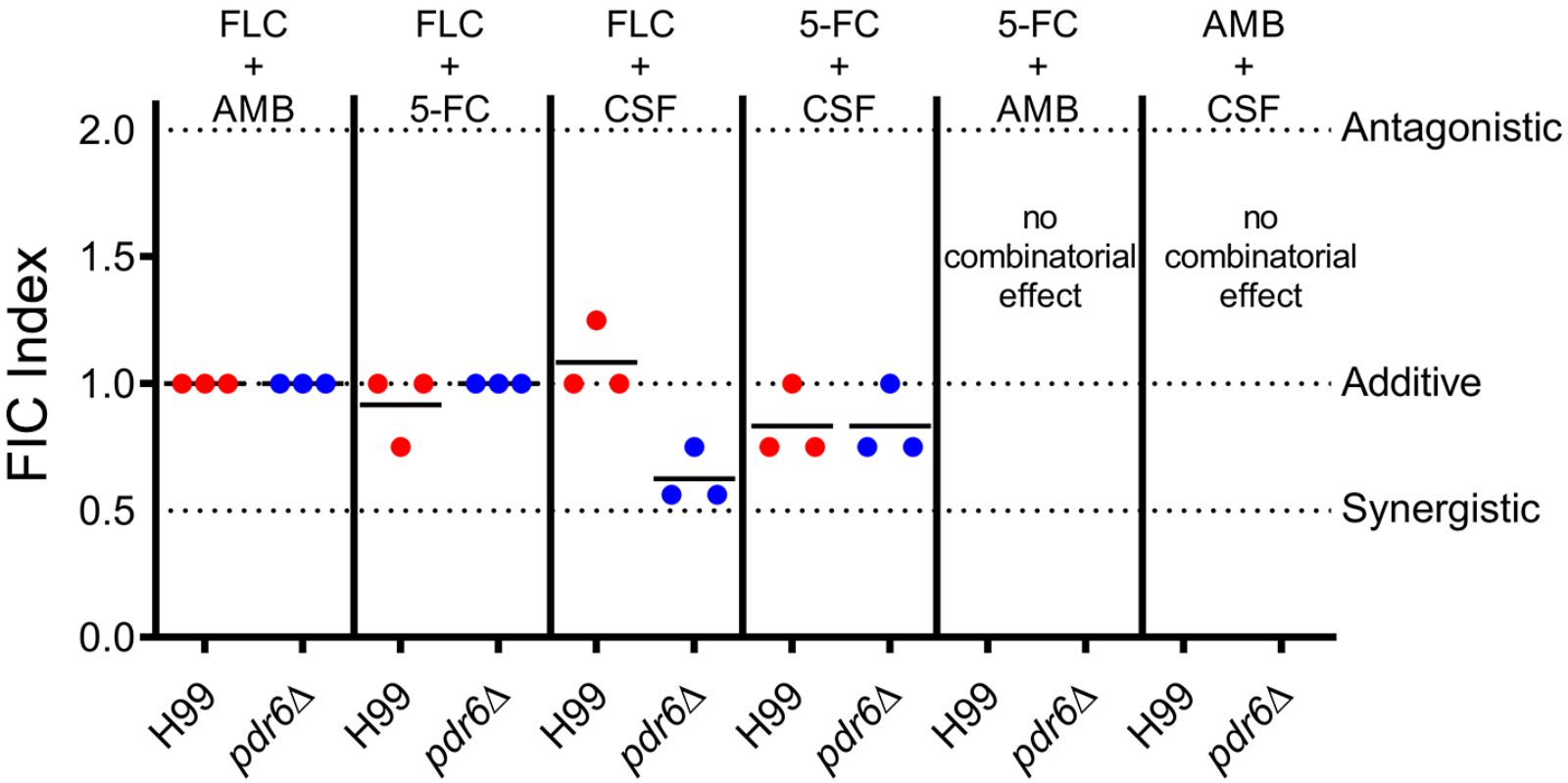
FLC + AMB
FLC + 5-FC
FLC + CSF
5-FC + CSF
5-FC + AMB
AMB + CSF
FIC Index
2.0
1.5
1.0
0.5
0.0
Antagonistic
Additive
Synergistic
no combinatorial effect
no combinatorial effect
H99
pdr6Δ
H99
pdr6Δ
H99
pdr6Δ
H99
pdr6Δ
H99
pdr6Δ
H99
pdr6Δ

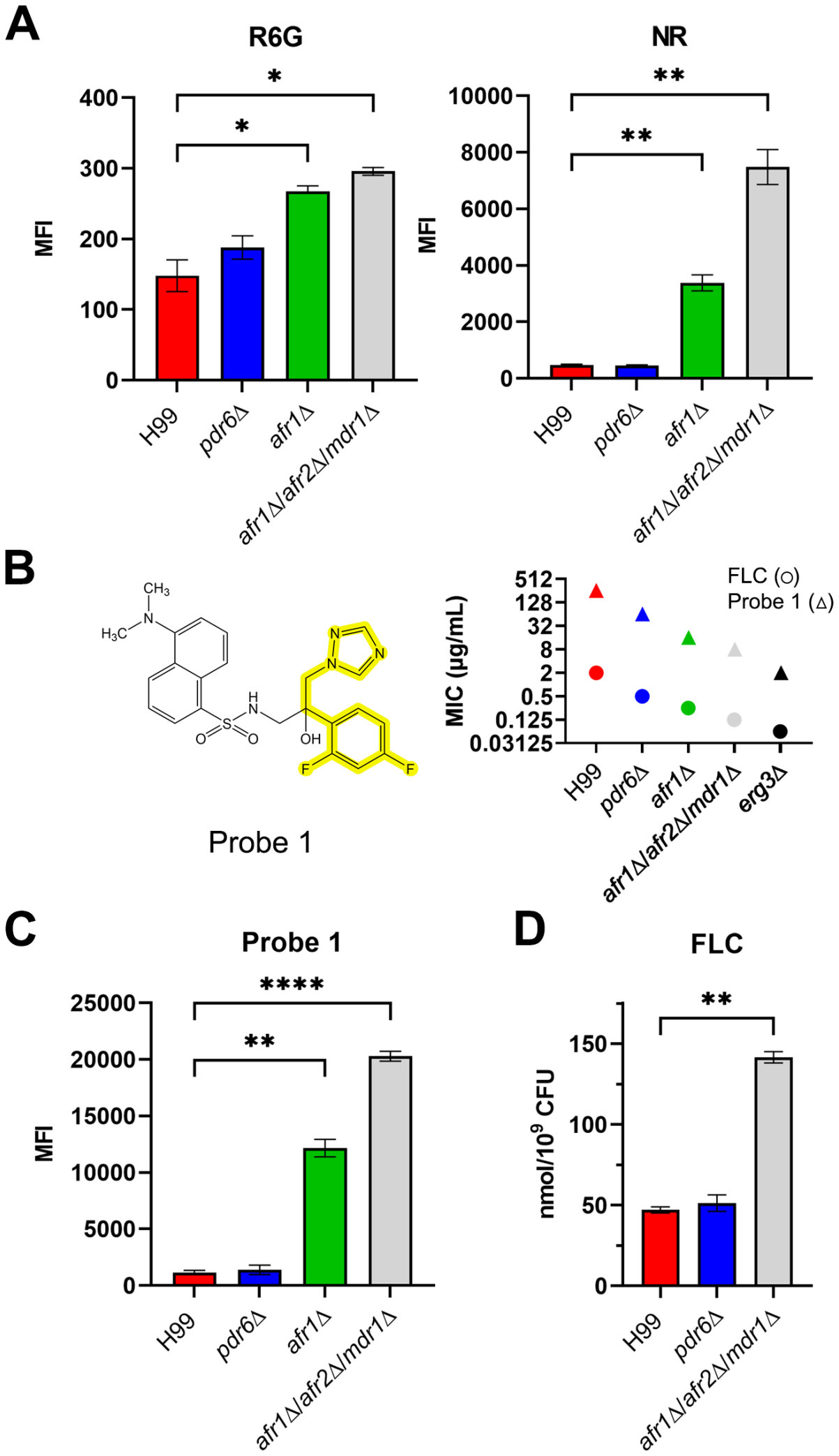
A
R6G
NR
MFI
400
300
200
100
0
10000
8000
6000
4000
2000
*
**
H99
pdr6Δ
afr1Δ
afr1Δ/afr2Δ/mdr1Δ
B
Probe 1
MIC (µg/mL)
512
128
32
8
2
0.5
0.125
0.03125
FLC (○)
Probe 1 (△)
erg3Δ
C
Probe 1
****
D
FLC
nmol/10^9 CFU
150
50

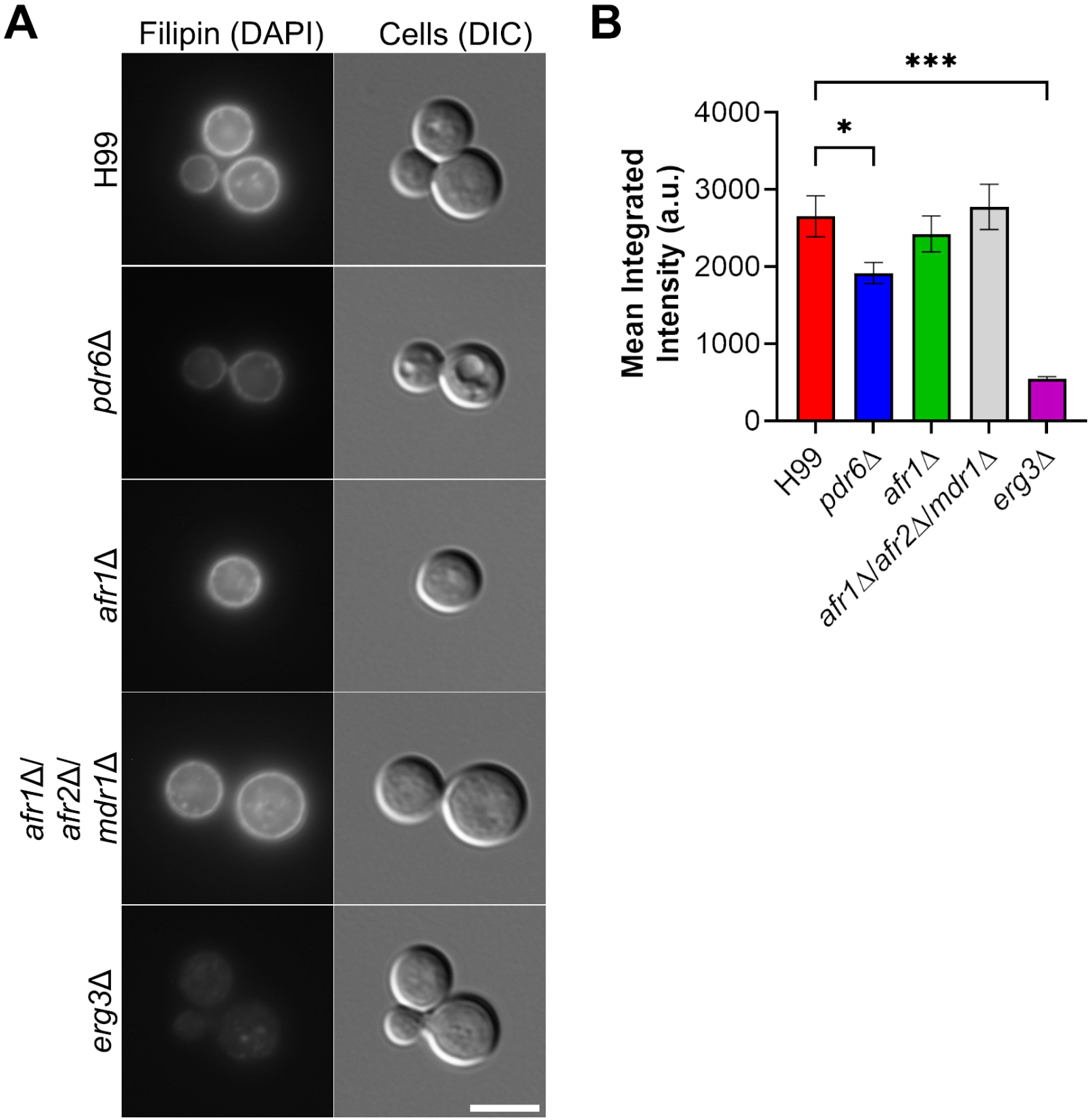
A
Filipin (DAPI)
Cells (DIC)
H99
pdr6Δ
afr1Δ
afr1Δ/
afr2Δ/
mdr1Δ
erg3Δ
B
***
*
Mean Integrated
Intensity (a.u.)
4000
3000
2000
1000
0
H99
pdr6Δ
afr1Δ
afr1Δ/afr2Δ/mdr1Δ
erg3Δ

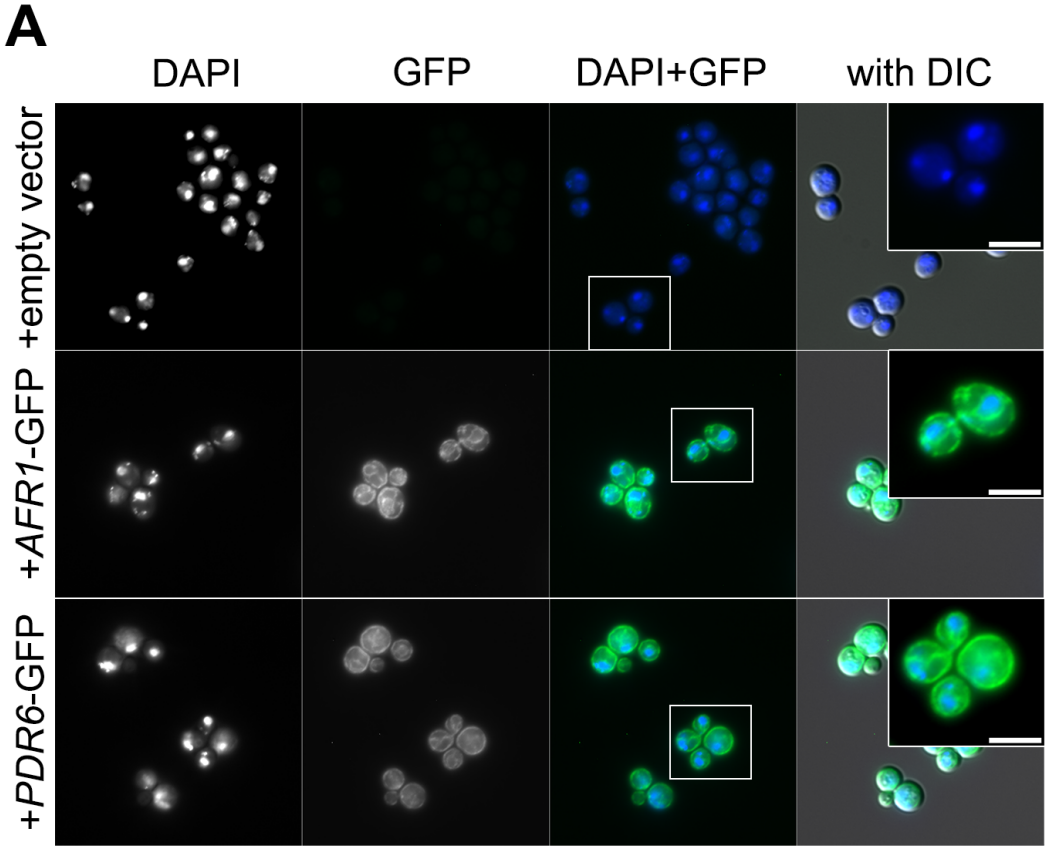
A
DAPI
GFP
DAPI+GFP
with DIC
+empty vector
+AFR1-GFP
+PDR6-GFP

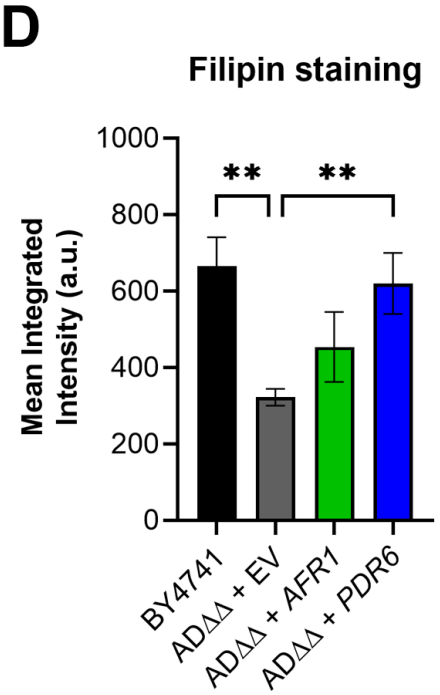
D
Filipin staining
Mean Integrated Intensity (a.u.)
1000
800
600
400
200
0
**
**
BY4741
ADΔΔ + EV
ADΔΔ + AFR1
ADΔΔ + PDR6

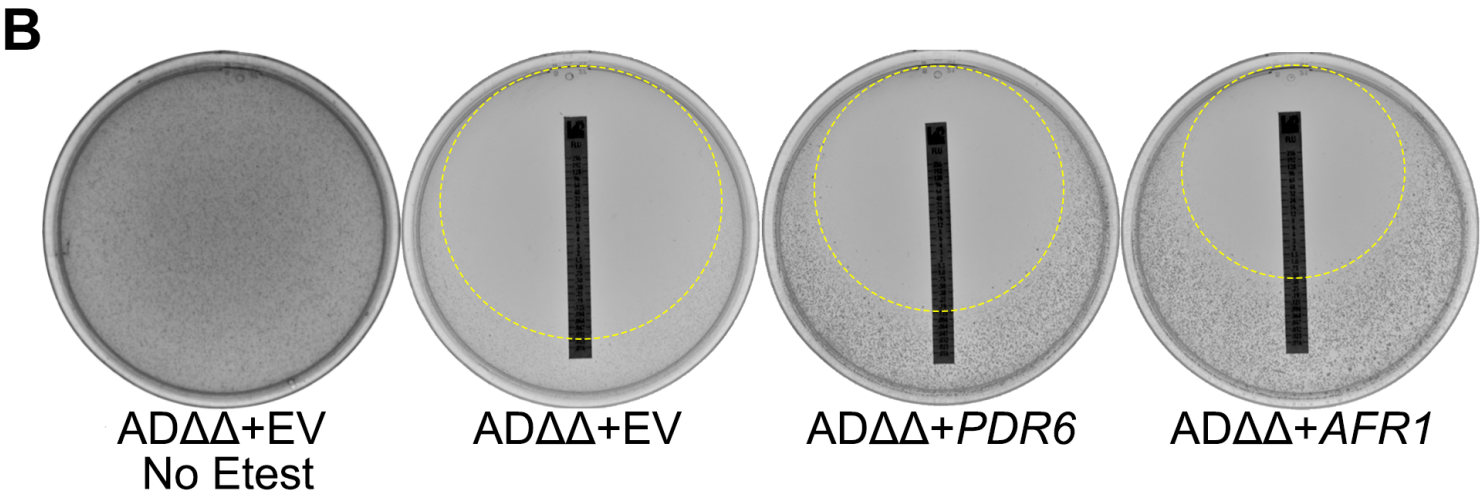
B
ADΔΔ+EV
No Etest
ADΔΔ+EV
ADΔΔ+PDR6
ADΔΔ+AFR1

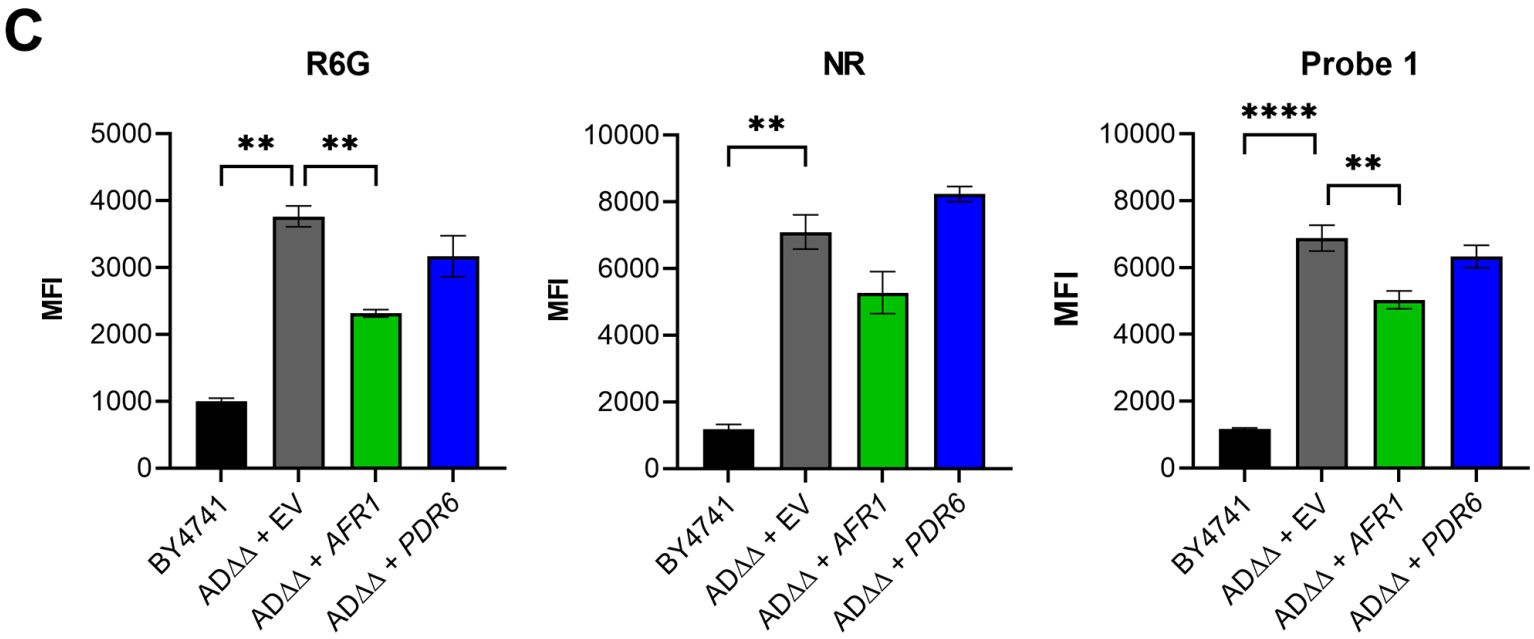
C
R6G
NR
Probe 1
MFI
5000
4000
3000
2000
1000
0
10000
8000
6000
4000
2000
0
**
**
**
****
**
BY4741
ADΔΔ + EV
ADΔΔ + AFR1
ADΔΔ + PDR6

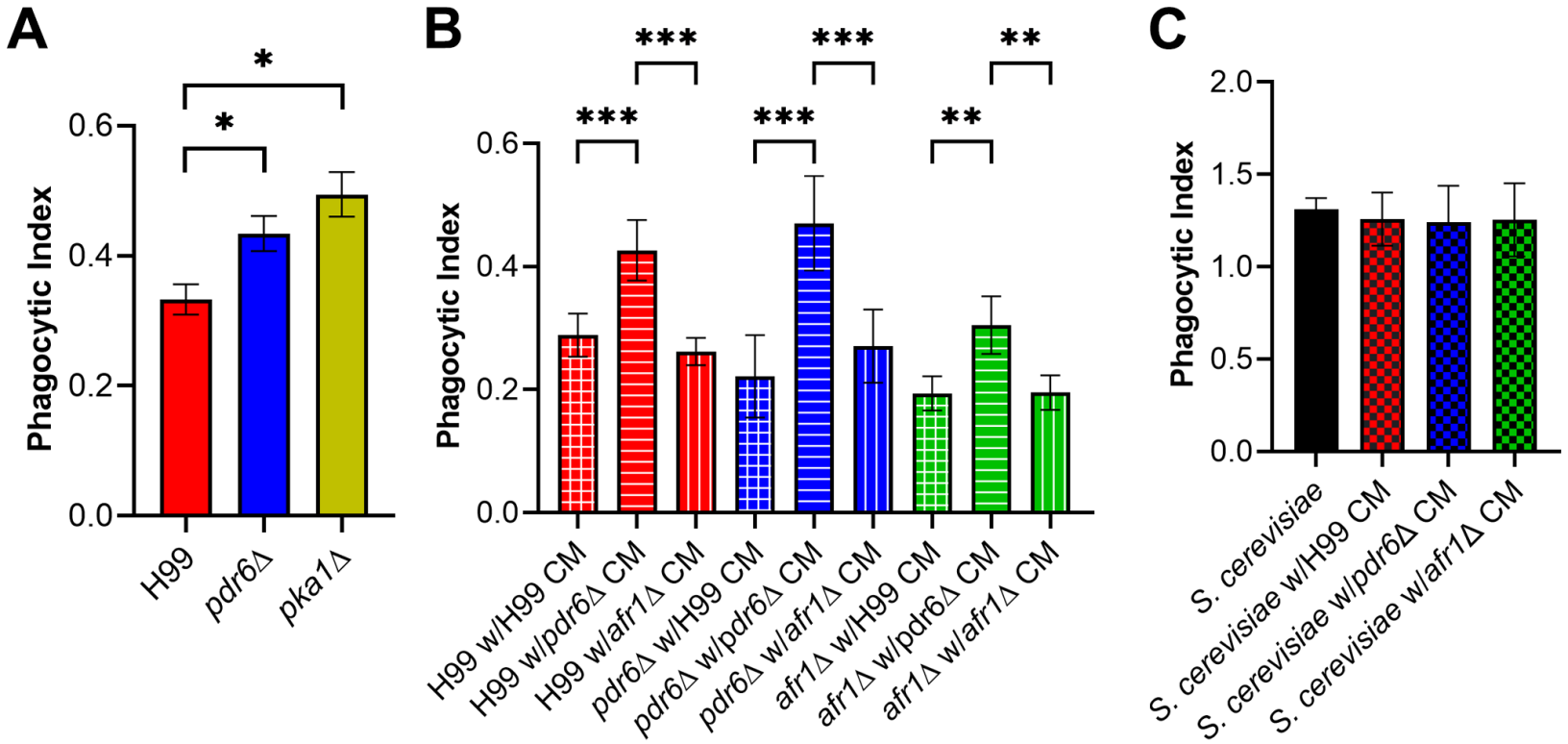
A
Phagocytic Index
0.0
0.2
0.4
0.6
*
*
H99
pdr6Δ
pka1Δ
B
Phagocytic Index
0.0
0.2
0.4
0.6
***
***
***
***
**
**
H99 w/H99 CM
H99 w/pdr6Δ CM
H99 w/afr1Δ CM
pdr6Δ w/H99 CM
pdr6Δ w/pdr6Δ CM
pdr6Δ w/afr1Δ CM
afr1Δ w/H99 CM
afr1Δ w/pdr6Δ CM
afr1Δ w/afr1Δ CM
C
Phagocytic Index
0.0
0.5
1.0
1.5
2.0
S. cerevisiae
S. cerevisiae w/H99 CM
S. cerevisiae w/pdr6Δ CM
S. cerevisiae w/afr1Δ CM

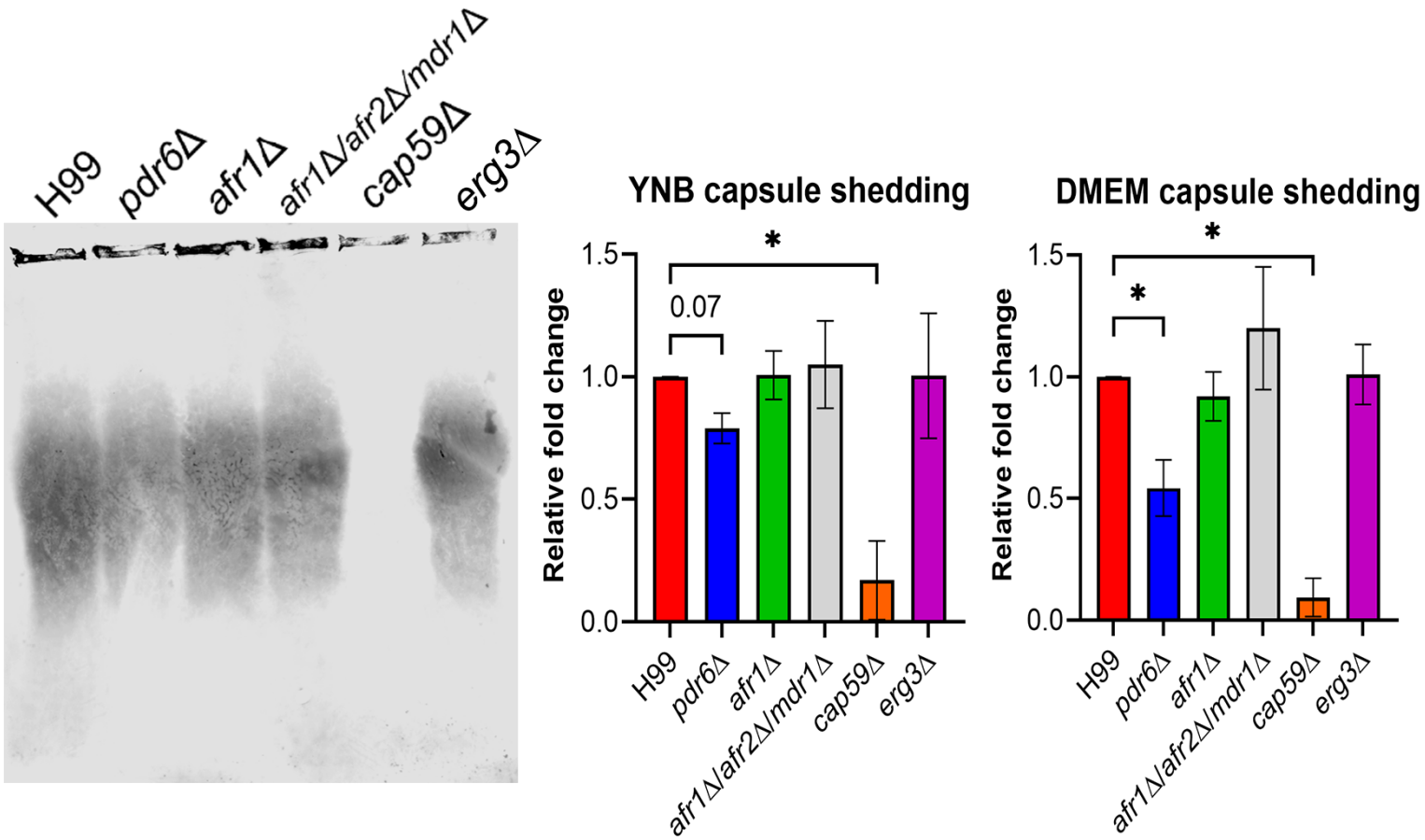
A
H99
pdr6Δ
afr1Δ
afr1Δ/afr2Δ/mdr1Δ
cap59Δ
erg3Δ
YNB capsule shedding
DMEM capsule shedding
Relative fold change
1.5
1.0
0.5
0.0
*
0.07
H99
pdr6Δ
afr1Δ
afr1Δ/afr2Δ/mdr1Δ
cap59Δ
erg3Δ

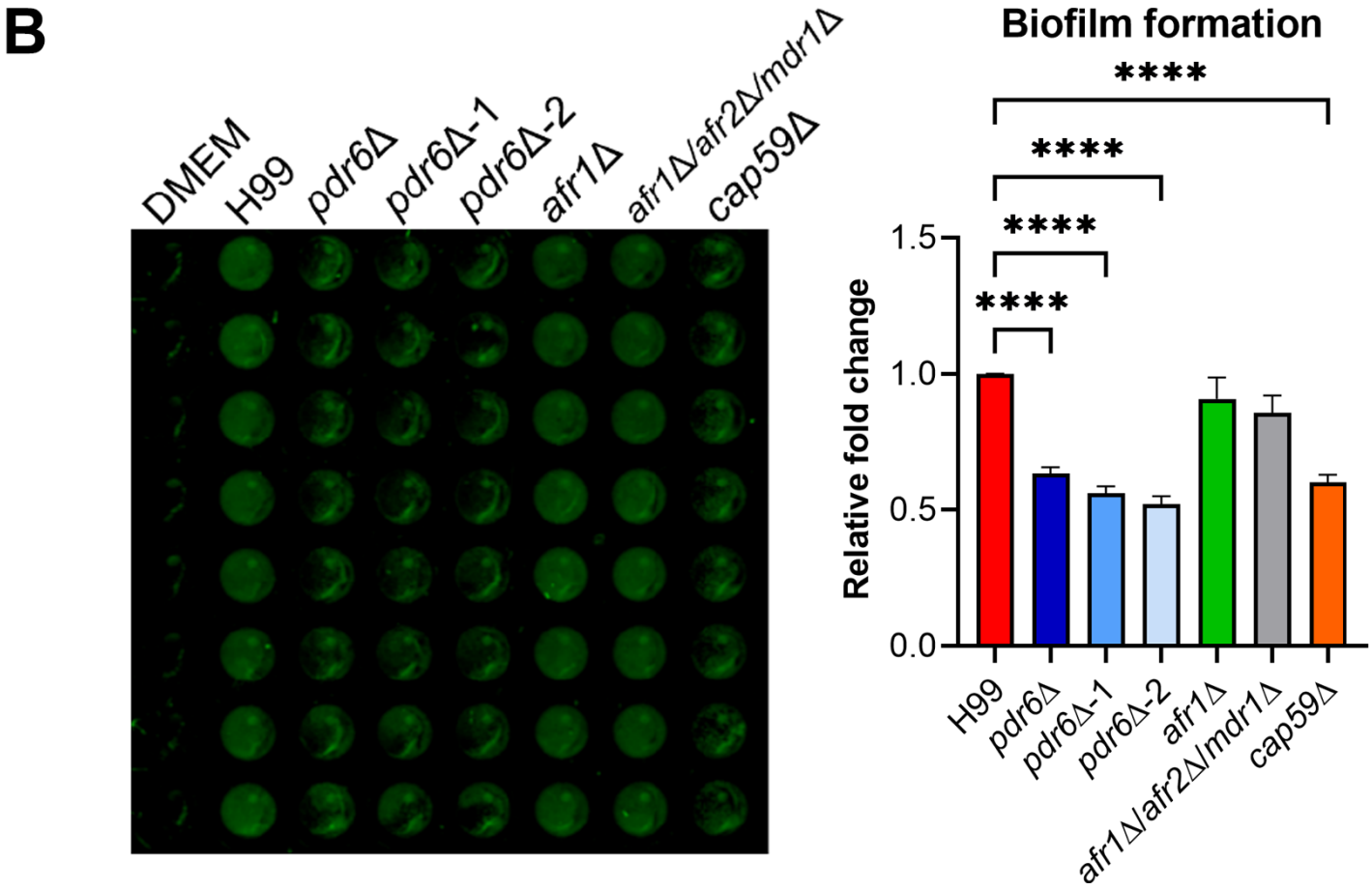
B
DMEM
H99
pdr6Δ
pdr6Δ-1
pdr6Δ-2
afr1Δ
afr1Δ/afr2Δ/mdr1Δ
cap59Δ
Biofilm formation
****
Relative fold change
1.5
1.0
0.5
0.0
H99
pdr6Δ
pdr6Δ-1
pdr6Δ-2
afr1Δ
afr1Δ/afr2Δ/mdr1Δ
cap59Δ

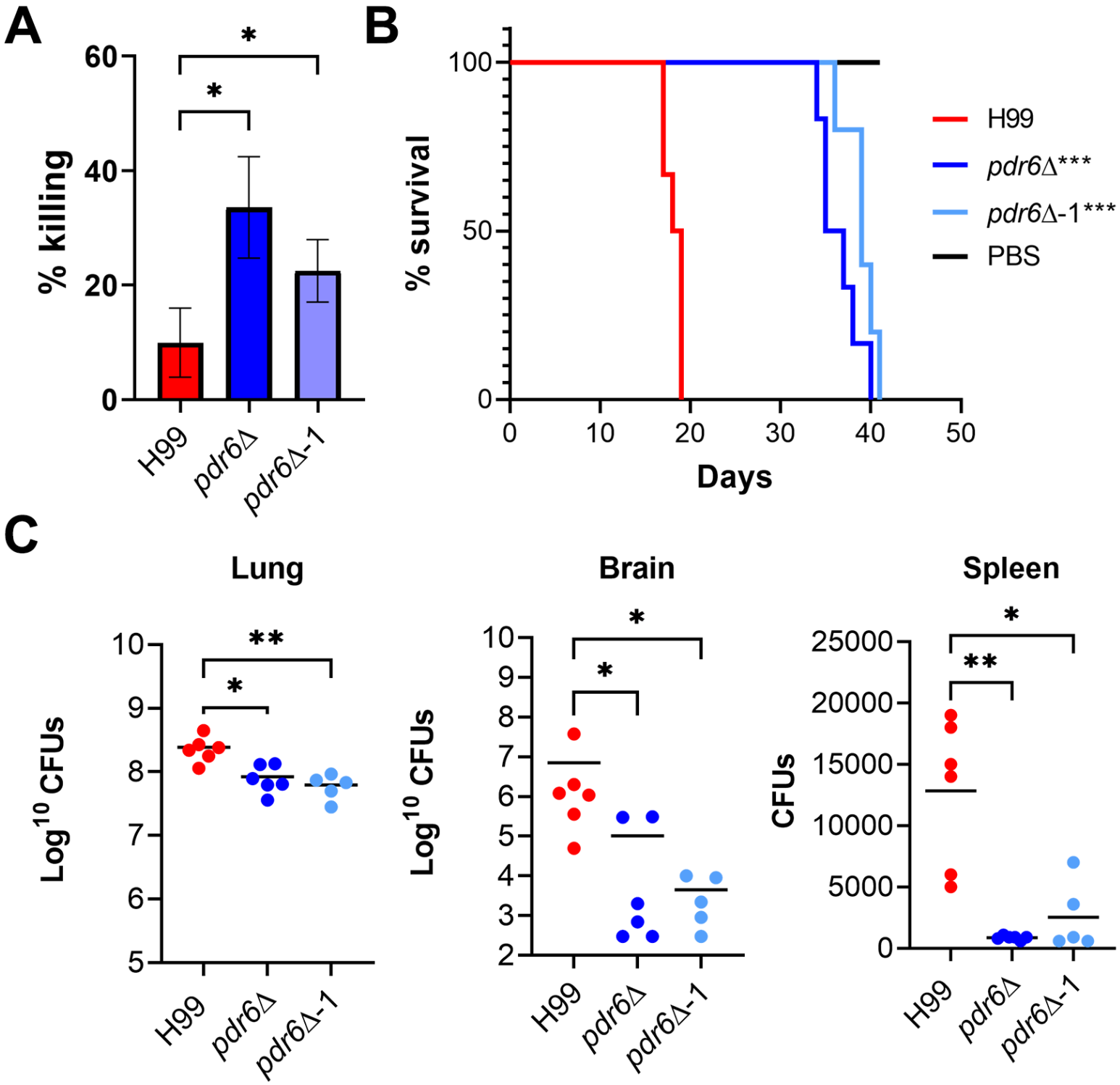
A
% killing
60
40
20
0
*
*
H99
pdr6Δ
pdr6Δ-1
B
% survival
100
50
0
0
10
20
30
40
50
Days
H99
pdr6Δ***
pdr6Δ-1***
PBS
C
Lung
Log10 CFUs
10
9
8
7
6
5
**
*
H99
pdr6Δ
pdr6Δ-1
Brain
Log10 CFUs
10
9
8
7
6
5
4
3
2
*
*
H99
pdr6Δ
pdr6Δ-1
Spleen
CFUs
25000
20000
15000
10000
5000
0
*
**
H99
pdr6Δ
pdr6Δ-1

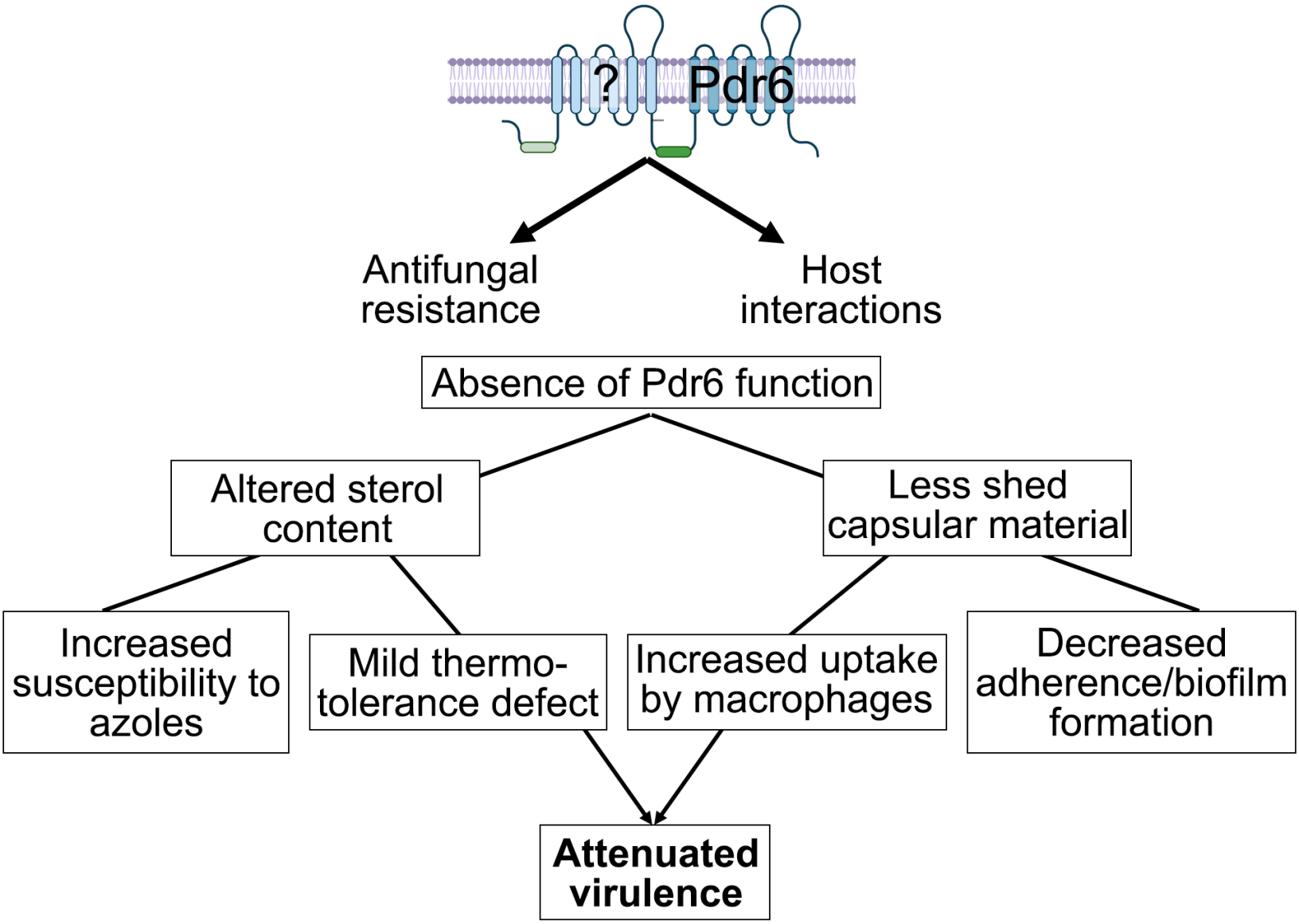
?
Pdr6
Antifungal resistance
Host interactions
Absence of Pdr6 function
Altered sterol content
Less shed capsular material
Increased susceptibility to azoles
Mild thermo-tolerance defect
Increased uptake by macrophages
Decreased adherence/biofilm formation
Attenuated virulence

TABLE 1 MICs of antifungals and xenobiotics.[a]

Strain	MICs (µg/mL)													
	FLC	ITC	VRC	KTC	PSC	AMB	5-FC	CHX	NOC	BER	PQ	TSA	MEN	CSF
H99	2	1	.0625	0.5	1	4	2	0.25	0.0625	8	12.5	2	16	32
***pdr6*Δ**	0.5 – 1	0.5 – 1	0.0156 – 0.0312	0.0625 – 0.125	0.25 – 0.5	4	4	0.25	0.0625	8	12.5	2	16	64
***afr1*Δ**	0.25	0.25 – 0.5	0.0156 – 0.0312	0.0312 – 0.0625	0.25	4	2	0.0156	0.0312 – 0.0625	8	12.5	0.5	16	64
***afr1*Δ/ *afr2*Δ/ *mdr1*Δ**	0.0625 – 0.125	0.125	0.0078 – 0.0156	0.0156	0.0625	4	4	0.0156	0.0312 – 0.0625	8	12.5	0.5	8	64
***erg3*Δ**	0.125 – 0.25	0.0625	0.0078	0.0312 – 0.0625	0.125	4	2	0.0625 – 0.125	0.0312	0.5	3.125	0.5	16	32

[a] b Values given are the range of MICs obtained from at least three independent experiments. FLC, fluconazole; ITC, itraconazole; VRC, voriconazole; KTC, ketoconazole; PSC, posaconazole; AMB, amphotericin B; 5-FC, 5-fluorocytosine; CHX, cycloheximide; NOC, nocodazole; BER, berberine; PQ, paraquat; TSA, trichostatin A; MEN; menadione; CSF, caspofungin.